

# Synthesis and thermodynamic of minerals

## Balitsky V. S., Shapovalov Yu. B., Balitskaya L. V., Balitsky D. V., Setkova T. V. Cr-containing topaz crystal growth on a seed in supercritical aqueous-fluoride fluids and some properties of as-grown crystals

Institute of experimental mineralogy of the Russian Academy of Sciences, Chernogolovka [balvlad@iem.ac.ru](mailto:balvlad@iem.ac.ru)

For the first time the Cr-containing topaz single crystals with unusual alexandrite effect and intensive fluorescence under influence of ultra-violet light are grown up. Growth conditions and the external and internal morphology of crystals and their physical properties is studied.

**Key words:** Cr-containing topaz, hydrothermal growth of crystals, morphology of crystals, physical properties of topaz

**Citation:** Balitsky, V. S., Yu. B. Shapovalov, L. V. Balitskaya, D. V. Balitsky, T. V. Setkova (2012), Cr-containing topaz crystal growth on a seed in supercritical aqueous-fluoride fluids and some properties of as-grown crystals, *Vestn. Otd. nauk Zemle, 4*,

**Introduction** The topaz, as it is known [Naumov, etc., 1977], is a polygene mineral. Its crystallisation is occurred in magmatic, pegmatic and hydrothermal stages of mineralization, covering a wide range of temperatures (from 250 to 900°C) and pressures (from 30 to 200 MPa). Conditions of topaz formation in the nature have been determined after many experimental and thermodynamic studies of its stability and mineral equilibriums. Experimental researches, as a rule, were accompanied by obtaining of microscopic crystals of topaz [Rosenberg, 1972; Balitsky et al., 2002]. The single crystals of topaz were never grown on seeds until recently. It is related to a limited practical application of the natural topaz only in jewellery which is extracted in sufficient quantity for the market requirements. The exception is the rarest and valuable form – Cr-containing topaz. The presented work is devoted to finding-out about conditions of crystal growth such kind of topaz.

### Technique, equipment and materials

At a choice of technique of single crystal growth of Cr-containing topaz the early results on experimental studies of its isothermal reactions with aqueous solutions of HF and KF (molarity from  $10^{-4}$  to 10m and from 0 to 1.0m, accordingly) in the range of 300-600°C and 100 MPa have been considered. It has allowed taking in account the stability field of topaz depending on concentration of the HF and KF in fluid [Shapovalov, 1988]. In particular, it has appeared, that for stability of topaz at the specified reactions the solutions should have a high concentration of HF ( $3 \cdot 10^{-3}$  –  $8 \cdot 10^{-1}$  m) and low concentration of KF ( $< 7 \cdot 10^{-3}$  m). It being known that with rise of temperature from 300 to 600°C the field of stability of topaz in the diagram  $\lg(m_{\text{HF}})$ - $\lg(m_{\text{KF}})$  is considerably narrowed and displaced to the area of higher concentration of HF. The boundary values of maximum concentration of KF change insignificantly and lay close to  $\lg(m_{\text{KF}}) = -2.0$ .

In the same time, the influence of thermobaric parameters and composition of fluids on streamline of silica and alumina was simultaneously found out at separate and simultaneous dissolution of quartz and topaz in hydrothermal fluids of various compositions under

thermo-gradient conditions at 500-780°C and up to 150 MPa [Balitsky, etc., 2006]. It has been found that the topaz in hydrothermal fluoride fluids under thermo-gradient conditions is always transferred from rather low temperature zone to high-temperature zone. It is connected to retrograde character of dissolution of topaz, i.e. the temperature factor of solubility (TFS) has a negative sign. Topaz dissolution becomes more intensive at excess of silica in the system. The behaviour of quartz in the same solutions is ambiguous and differs from behaviour of topaz: at low density of fluid (less than  $0.4 \text{ g/cm}^3$ ) quartz is characterised by retrograde solubility. The silica in such fluids is similar to the alumina transfer which goes to high-temperature zone. But in more dense fluids the TFS of quartz becomes positive and dissolved silica is moving from hotter zone to less hot zone.

The growth of single crystals of topaz was realised in autoclaves of  $280 \text{ cm}^3$  made from Cr-Ni alloy A437b. The autoclaves were heated in a group electric furnace with two-section resistant heaters. The duration of runs was 30-60 days. The crystals were grown at temperatures from 500 to 780°C, pressures from 20 to 180 MPa. The difference of temperatures between bottom and top ends of autoclaves was from 20 to 100°C. The pressure and density of fluid in autoclaves were estimated by filling factors on  $P$ - $V$ - $T$  diagrams of pure water [Naumov, etc., 1971]. The temperature control was carried out by means of the thermo-measuring device Termodat - 25M1 equipped by chromel-coupe thermocouples with accuracy  $\pm 2^\circ\text{C}$ .

The initial solutions were prepared on basis of bi-distilled water and aluminium fluoride ( $\text{AlF}_3$ ) which were placed in the bottom of autoclave. The fluoride fluid was formed at heating of autoclave at the expense  $\text{AlF}_3$ . The chrome admixture was not specially added into autoclave, since it came to solution at rather insignificant dissolution of Cr-Ni body of autoclave. Topaz crystal growth was carried out on seed plates of  $2 \div 4 \times 6 \times 50 \div 70 \text{ mm}$ , cut out parallel to faces  $\{001\}$ ,  $\{110\}$  and  $\{120\}$  of natural topaz crystals from Volynsk deposit (Ukraine). Seeds were placed in the bottom zone of autoclave with help of copper wire. Nutrient, consisting of mix of fragments of topaz of 10-12 mm in diameter and synthetic quartz of ZY- and ZX-bars of  $2 \times 4 \times 30 \div 50 \text{ mm}$ , was placed in the top zone of autoclave. For creation of more contrast temperature gradient, the nutrient and seed zones were separated from each other by diaphragm of 10-15%.

Morphology and internal structure of as-grown crystals were studied by binocular (MBS-9) and polarising (Amplival po - d) microscopes; optical characteristics were defined by immersion method. The chemical composition was defined by microprobe analyser CamScan MV2300. X-ray characterisation was carried out by diffractometry on ADP2-01 Co at wavelength  $1.79021 \text{ \AA}$ . The luminescence of topaz was observed under a standard mercury lamp and UV laser EnSpectrR532 with recording of spectrum. The influence of ionizing irradiation on the as-grown topaz crystals was studied by  $\gamma$ -irradiation ( $^{60}\text{Co}$ , 5 Mrad.) and under irradiation by linear electron accelerator (12 Mv).

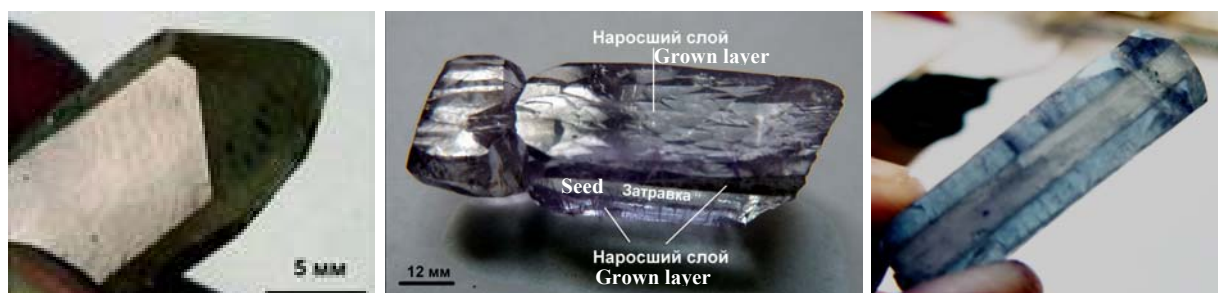


Fig. 1. Morphology of single crystal of Cr-containing synthetic topaz

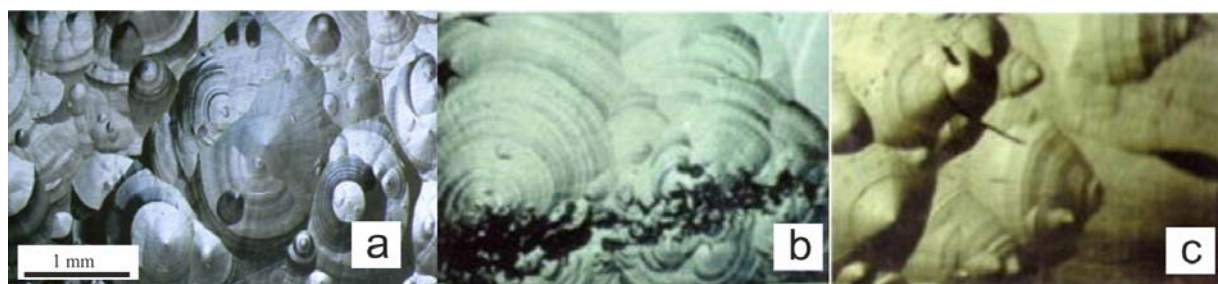


Fig. 2. Vicinal relief of faces of pinacoid {001} (a), prisms {101} (b) and bi-pyramid {113} (c) of synthetic Cr-containing topaz

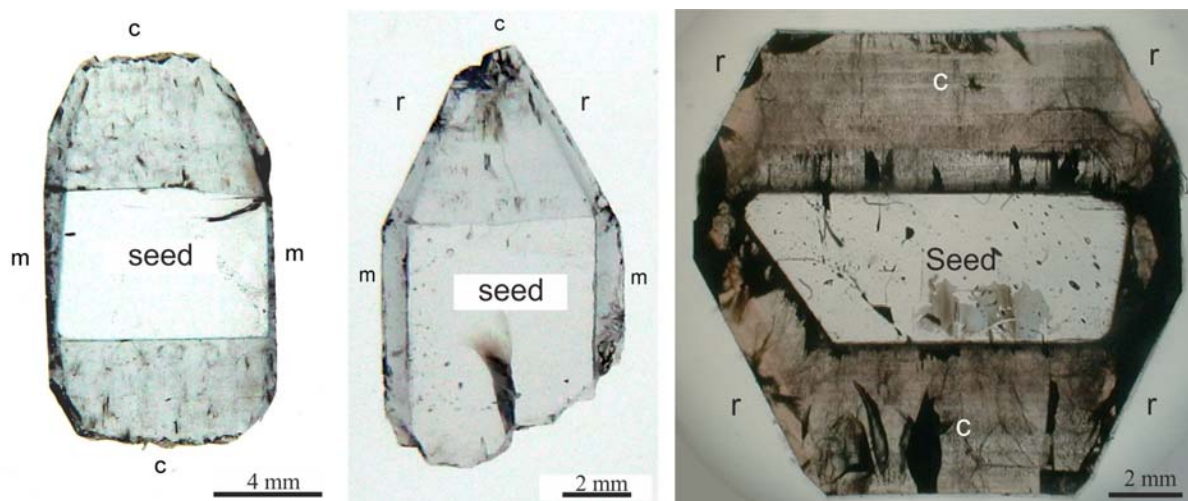


Fig. 3. Internal sectorial-zone structure of synthetic Cr-containing topaz



Fig. 4. Colour of synthetic Cr-containing topaz at day (a), fluorescent lamp (b) and UV (c) illumination

**Results and discussion** The most intensive growth of topaz is fixed in [001] direction at 700-730°C as at low (10–20 %), and at high (40-50 %) fillings of autoclaves (pressure in order of 40–70 and 150–200 MPa, accordingly). Absolute values of growth rates did not exceed the first tenth of millimetre per day. Almost all faces known for natural topaz crystals were observed on as-grown crystals (pinacoid {001}, prisms {110}, {120}, rhombohedrons {111}, {021}, etc.) (Fig. 1). Their surface, as a rule, is smoothed or covered by growth hillocks of regular and complex shape often with distinct concentric layers (Fig. 2a,b,c).

Irrational surfaces of growth are rough; their relief is combined by rhombohedrons and prismatic pyramids with cross-section size of 0.5 mm. The crystals are characterised by the distinct sectorial-zone structure revealed in cross-section cuts, by reason of changing in the direction of zones, which are parallel to certain faces (Fig. 3). The zones are often decorated by presence of numerous primary fluid inclusions with the size from thousand to tenth shares of millimetre. Besides sectors and growth zones, sometime, a thin fibrous structure of the grown layers is observed under polarised light. It was induced by regenerating growth mechanism of some faces. As-grown layer of the topaz crystals has a primary bluish-green colouring (Fig. 4a).

Like a natural topaz, the synthetic topaz is colored to intensive red-brown under ionising irradiation which disappears after heat treatment at 200-250°C. The microprobe X-ray analysis has shown a concentration of Cr in as-grown layers of topaz up to 0.5 mass%. The green-bluish colour of as-grown topaz crystals changes to red-violet under fluorescent lamp (Fig. 4b), and to brightly red colour under UV. Optical and fluorescence spectra specify that primary colouring of the topaz crystals is related to isomorphic occurrence of Cr<sup>3+</sup> in structure.

**Conclusion** Thus, the single crystals of Cr-containing topaz were grown for the first time. Crystals possess unusual alexandrite effect which is manifested by change of green-bluish colour at daylight to red-violet under fluorescent lamp illumination. The grown crystals are characterised also by intensive fluorescence of red colour under UV irradiation.

#### References:

- Balitsky, V. S., D. V. Balitsky, S. D. Balitsky, K. Aurisichio, M. A. Roma (2006). Peculiarities of streamline of silica and alumina in supercritical aqueous fluids and growing of topaz single crystals, *Geochemistry*, N 2, pp. 204–211 (in Russian).
- Naumov, G. B., B. N. Ryzhenko, I. L. Hodakovskiy (1971). The handbook of thermodynamics. M: Atomizdat, pp. 240.
- Naumov, V. B., V. I. Kovalenko, G. F. Ivanova, N. V. Vladykin (1977). Genesis of topaz according to studying of microinclusions, *Geochemistry*, № 3, pp. 323–340 (in Russian).
- Shapovalov, Yu.B. (1988). Mineral equilibria in the system K<sub>2</sub>O–Al<sub>2</sub>O<sub>3</sub>–SiO<sub>2</sub>–H<sub>2</sub>O–HF at T=300–600°C and P=1000 bar, Review on physical-chemical petrology, V.15, p. 160–167.
- Balitsky, V. S., L. T. Balitskaya, J. E. Shigley. (2002). Experimental study of the simultaneous dissolution and growth of quartz and topaz, *Journal of Crystal Growth*, T. 237-239, № 1-4, pp. 833-836.
- Rosenberg, P. E. (1972), Compositional variations in synthetic topaz, *American Mineralogist*, v. 56, pp.168–187.

## Barenbaum<sup>1</sup> A. A., Ablya<sup>2</sup> E.A. Physical evidence of abiogenic synthesis of oil hydrocarbons

<sup>1</sup>Institute of Oil and Gas Problems RAS, Moscow

<sup>2</sup>M. V. Lomonosov Moscow State University, Department of Geology, Moscow [azary@mail.ru](mailto:azary@mail.ru)

On the basis of the study a fetch from 21 sample of oil is established that the molecular- mass distribution of n-alkanes in oil well described by the Anderson-Schulz-Flory formula that used in the theory of polycondensation synthesis of hydrocarbons. It is shown that the distribution of n-alkanes in the oils is identical to their distribution in the products of the Fischer-Tropsch on catalysts of Fe<sub>2</sub>O<sub>3</sub>. It is concluded that a significant portion of petroleum hydrocarbons are generated in the upper floors of the Earth's crust in processes of the polycondensation.

**Key words:** Oil, hydrocarbons, n-alkanes, formula Anderson-Schulz-Flory, polycondensation synthesis, molecular mass distribution

**Citation:** Barenbaum, A. A, E. A. Ablya, (2012), Physical evidence of abiogenic synthesis of oil hydrocarbons, *Vestn. Otd. nauk Zemle, 4*

It is known that oil and gas hydrocarbons may be formed as a result of destruction of bioorganic molecules, and as a result of processes of abiogenic synthesis. On this basis, it is suggested that oil and natural gas on the Earth origin from dead organic matter contained in the rocks – the organic hypothesis [Kontorovich, 1998], or they occurred in polycondensation synthesis reactions of hydrocarbons from carbon oxides and hydrogen, are part of the underground fluids and gas occurring in the terrestrial depths – the mineral hypothesis [Journal, 1986]. Also there is the views [Dmitrievsky, 2008] that oil and gas born with the participation of both biogenous and abiogenous mechanisms of hydrocarbons formation.

In accordance with the results of [Barenbaum, 2004], the hydrocarbons of oil and gas are formed mainly in two ways: 1) in the reactions of polycondensation synthesis of hydrocarbons on the catalysts included in rock formation, and 2) by means of the extraction of hydrocarbons formed in the processes of diagenesis and catagenesis organic substance of sedimentary rocks by underground fluids and waters.

The first process determines presence into oil the normal alkanes, alkanols, and other relatively simple structured hydrocarbon. The second is responsible for presence into the oil a much more complex carbon-containing compounds, including the biomarkers are structurally relating with organic matter from which they originated, as well as hydrocarbons, which have experienced changes during biodegradation processes [Petrov et al., 1994].

Biomarkers serve irrefutable proof of participation destruction processes of dead organisms of sediment rocks in formation of the oil. By means of biomarkers can be judged about geological conditions of formation and the conversion degree of the original organic substance, on the conditions of formation of oil and gas, as well as solve other tasks [Bazhenova et al., 2000].

The share of biomarkers in untransformed oils, however, is insignificant; it usually does not exceed a few percent. The bulk of oil hydrocarbons (primarily aliphatic) have not a pronounced structural connection with the organic substance of sedimentary rocks. The formation of these hydrocarbons can in principle be explained due to biogenous and abiogenous mechanisms of their genesis. The choice between these alternatives has long served as a

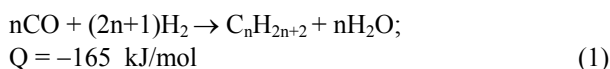
## Abstracts

point of contention of supporters of organic and mineral hypotheses origin of oil and gas.

The well-defined evidences syntheses of oil hydrocarbons, however, are absent. Attracted to this argument, such as atypical agents to isotope ratio  $C^{13}/C^{12}$  in some oil and gas, the absence in many cases the "mother bed of oil", accumulations are confined to a "channels of degassing" or placing their deposits in the crystalline basement, etc. were indirect. These facts cannot be reliable evidence of abiogenous synthesis hydrocarbons of oil.

In the present work we are proving the involvement of abiogenous synthesis oil hydrocarbons on base of study the molecular weight distribution of normal alkanes in the raw oils. This group is usually dominant in the raw oil type of A1 on the classification Petrov [Petrov *et al.*, 1994], which did not undergone biodegradation. The content n-alkanes in such oil, in contrast to biomarkers, can reach tens of percent.

Normal alkanes are the core group of hydrocarbons synthesized from the oxides of carbon and hydrogen in many polycondensation reactions [Rudenko, 1969] and, in particular, in the simplest of them, in the Fischer-Tropsch synthesis (FT-synthesis):



where:  $C_nH_{2n+2}$  – notations of n-alkanes, Q – enthalpy, "minus" indicates the exothermic reaction nature.

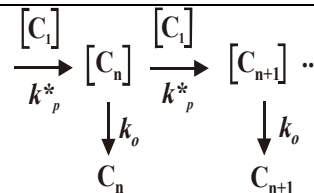
In contrast to other polycondensation reactions, today Fischer-Tropsch synthesis found application in the industrial production of hydrocarbons. Therefore now it has been well studied theoretically and experimentally. Analysis of the distributions of hydrocarbons in products FT-synthesis consisting primarily of alkanes, alkenes, alkanols and alkanaley with number carbon atoms in the chain of 1 to 100 and above, shows that in many cases these distributions obey the classical equation of the Anderson-Schulz-Flory [Glebov, Kliger, 1994]:

$$\lg(g_n/n) = \lg(\ln^2\alpha) + n \cdot \lg\alpha \quad (2)$$

where:  $g_n$  – the mass fraction of hydrocarbons with n carbon atoms in molecules,  $\alpha$  – constant factor ( $0 < \alpha \leq 1$ ).

The equation (2) has been obtained by G. Schultz (Schulz, 1935) for the molecular mass distribution of polymers in processes radical polymerization. For such polymers obtained by linear polycondensation P. Flory (Flory, 1936) proposed the close equation. American chemists G. Henritsi-Olive and S. Olive [Henritsi-Olive, Olive, 1987] used this formula for the products of Fischer-Tropsch and they found that for values  $\alpha > 0.5$ , formula (2) also well describes the distribution of individual monokomponent FT-synthesis which been installed by R. Anderson (Anderson *et al.*, 1951).

Thus, it became clear that equation (2) reflects a universal physical-chemical process of grow chain hydrocarbons that bears a probabilistic nature. Equation (2) is theoretically explained [Glebov, Kliger, 1994] by means a number of assumptions based on the pattern formation of polymers:



where:  $[C_1]$ ,  $[C_n]$ ,  $[C_{n+1}]$  – the concentration of intermediates with number of carbon atoms on catalyst surface 1, n and n+1;  $k_p$  and  $k_o$  – the rate of growth and breakage of the carbon chain, respectively.

These conditions as applied to the synthesis of n-alkanes are: 1) the increment of hydrocarbon chain occurs in result of accidental accession  $[C_1]$ -intermediate (molecule  $CH_2$ ), 2) the chain undergoes by a random breakage, and 3)  $k_p$  and  $k_o$  are constants which do not depend on chain length.

It this case formula (2) describes a molecular-mass distribution of polycondensation products, where the parameter  $\alpha$  has a physical meaning:

$$\alpha = k_p / (k_p + k_o) \quad (3)$$

Equation (2) and its modifications are now turned into an effective tool for studying mechanisms formation of hydrocarbons in the FT-synthesis [Glebov, Kliger, 1994].

The applicability of the formula (2) for n-alkanes of oil for the first time has been demonstrated Glebov [Glebov, 2002]. Barenbaum [Barenbaum, 2007] indicated the possibility of its application in other cases as well as suggested the advisability of its use at analyzing the composition of hydrocarbon in aquamarine gas-hydrates. These studies, however, were only preliminary.

The present work aims to extending the Anderson-Schulz-Flory model, to include the rationale for the possibility of polycondensation of the simplest hydrocarbon of oil.

To this end we studied and systematized the distribution of n-alkanes into 21 samples of "crude" oil type A<sub>1</sub>. Investigations were carried out on chromatograph Trace Ultra Thermo Finnigan, on a column of a Sol-Gel 1-MS with a neutral phase, column length 60 m and diameter 0.25 mm, layer of 0.25 nm, temperature of the detector 320°C and the evaporator 300°C, temperature mode is 3°C/min. Verification and identification of hydrocarbons with high-resolution was on performed spectrometer Thermo Finnigan MAT 900 (with chromatograph Trace GC) with the same column and at the same temperature regime.

We investigated oils of various deposits in the Early Paleozoic sediments, which mainly were at depths exceeding 2 km. The average weight of oil was 0.85 g/cm<sup>3</sup>. Content of the polar fractions in the group composition of oil did not exceed 10%. The methane hydrocarbons of normal structure (80%) and the aromatic hydrocarbons are dominated. Also were investigated very light oil consisting mainly of hydrocarbons of the normal range.

The distributions n-alkanes in the oils were analyzed in a semilogarithmic coordinate system equation (2), starting the number of carbon atoms in the molecule  $n = 10$  (Fig. 1a). The normalized results of the measurements were processed by least squares method which allowing to assess in what degree the distribution n-alkanes in oil fit with the theoretical dependence (2) as well as allowing to determine the coefficient  $\alpha$ .

Based on formula (2) the value of parameter  $a$  can be found in two independent ways: 1) from the tangent of angle slope of the line in Fig. 1a to the x-axis and 2) using the length of line segment that she intercepted on the ordinate. In the cases when chromatograms contain information on all n-alkanes of oil, including gas and

gasoline fractions, values of parameter  $\alpha$ , calculated by both methods agree well with each other [Glebov, 2002].

In our case we calculated the value of the parameter  $a$  from the slope of the line to the abscissa. The processing results are shown in Table 1.

Analysis of the data in Table 1 leads to the following conclusions.

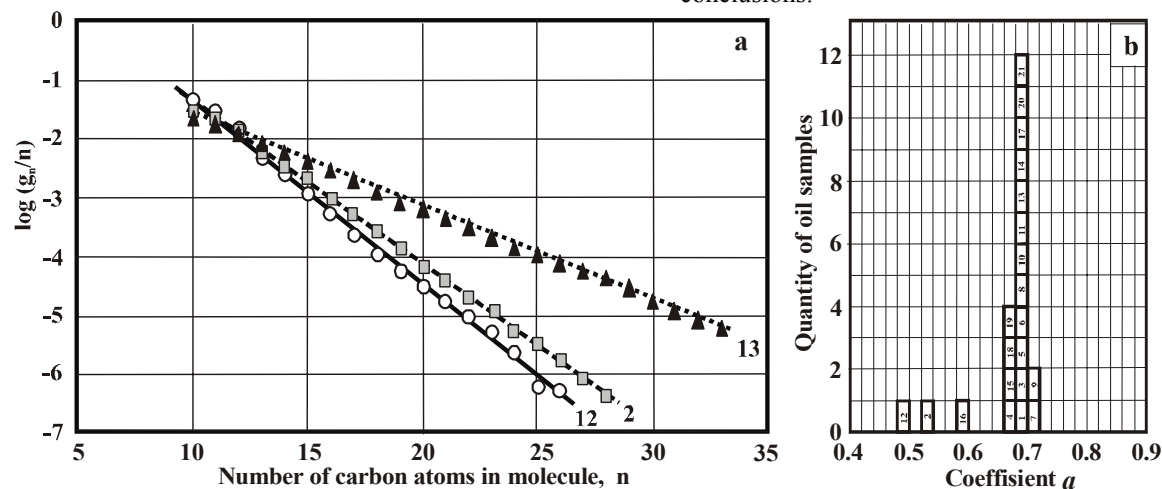


Fig. 1. a) Molecular-mass distribution of normal alkanes three samples of oil in the coordinate system of the Anderson-Schulz-Flory equation and b) distribution of coefficient  $\alpha$  for oils. Numerals are numbers of oil samples in Table 1.

Table 1. The results of processing of chromatograms of crude oils

No of ampl	Tangent of angle inclination line on Fig. 1a	Length of line on the ordinate	Coefficient of determinacy	Value of coefficient $\alpha$
1	-0.1576	-0.0280	0.9963	0.696
2	-0.2783	+1.4311	0.9995	0.527
3	-0.1629	+0.0625	0.9982	0.687
4	-0.1694	+0.1106	0.9990	0.677
5	-0.1656	+0.0893	0.9979	0.683
6	-0.1675	+0.0117	0.9931	0.680
7	-0.1515	-0.1259	0.9990	0.705
8	-0.1634	+0.0207	0.9977	0.686
9	-0.1465	-0.2715	0.9715	0.714
10	-0.1669	+0.0244	0.9960	0.681
11	-0.1595	+0.0487	0.9949	0.693
12	-0.3115	+1.7538	0.9966	0.488
13	-0.1575	-0.0260	0.9989	0.696
14	-0.1644	+0.0585	0.9990	0.685
15	-0.1691	+0.1142	0.9986	0.677
16	-0.2264	+0.6971	0.9952	0.593
17	-0.1559	-0.0361	0.9985	0.698
18	-0.1732	+0.1789	0.9979	0.671
19	-0.1698	+0.1381	0.9989	0.676
20	-0.1670	+0.1080	0.9984	0.681
21	-0.1603	+0.0082	0.9990	0.691

1. Molecular-mass distribution of n-alkanes in the oils with high precision (coefficient of determination over 0.99) is described by the Anderson-Schulz-Flory formula characterizing the hydrocarbons of polycondensation synthesis.

2. The value of the parameter  $a$  lie ranges from 0.488 to 0.714, forming a sharp maximum at  $\alpha = 0.69$  (Fig. 1b). The samples 2, 12 and 16 differing from the general pattern. They are characterized by a greater slope distributions of hydrocarbons. According to its physical

properties we have classified all three samples as condensate rather than as oil.

3. Comparison of the distributions of n-alkanes in crude oils and products FT-synthesis shows that for ours oils the average value parameter  $\alpha = 0.69$  is almost identical to the experimentally obtained in the FT-synthesis on catalysts from  $\text{Fe}_2\text{O}_3$ , at temperatures of 150–300°C [Glebov, Kliger, 1994]. In experiments the temperature and pressure as well as the composition of synthesis gas (the ratio of  $\text{H}_2$  to  $\text{CO}$ ) at comparable amounts of  $\text{CO}$  and  $\text{H}_2$  affected on the value parameter  $\alpha$

weakly. The value of this parameter  $\alpha$  decreased, when hydrogen is sharp prevail.

A similar increase in the steepness of molecular-mass distribution of n-alkanes observed in crude oils and condensates at depths of more than 3–4 km [Sokolov, Abliya, 1999].

Thus, according to the present materials and the results of [Barenbaum, 2004, 2007] suggest that: 1) significant portion of oil hydrocarbons can be generated in the processes of polycondensation synthesis and 2) hydrocarbons of oils forming in the upper floors of the earth's crust rather than in the depth of the mantle, where sustainable the existence of hydrocarbons is problematic [Melenevsky, Kontorovich, 2007].

*References:*

1. Barenbaum, A A (2004). The mechanism of formation of oil and gas fields, *Doklady Akademii Nauk*, V.399, №6, pp. 802–805.
2. Barenbaum, A. A. (2007). On possible relationship between gas-hydrates and submarine groundwater, *Water Resources*, V.34, №5, pp.587–592.
3. Bazhenova, O. K., Yu. K. Burlin, B. A. Sokolov, V. E. Khain (2000). *Geochemistry and geology of oil and gas*, Moscow State University Press, 384 p (in Russia).
4. Dmitrievsky, A. N. (2008). Polygenesis of oil and gas, *Doklady Akademii Nauk*, V.419, №3, pp. 373–377.
5. Glebov, L. S. (2002). Molecular weight distribution of n-paraffins Tengiz oil, *Neftekhimiya*, V.42, №2, pp. 92–94.
6. Glebov, L. S., G. A. Kliger (1994). Molecular weight distribution of the products of the Fischer-Tropsch, *Uspekhi khimii*, V.63, №2, pp. 192–202.
7. *Journal of the All-Union Chemical Society named DI Mendeleev* (1986). V.31, №5 (in Russia).
8. Henrizi-Olive, G., S. Olive (1987). *Chemistry of Catalytic Hydrogenation of CO*, Moscow: Mir, 248 p (in Russia).
9. Kontorovich, A. E. (1998). The sedimentary-migration theory oil-genezis. The status at the turn of XX and XXI centuries, the ways of further development, *Gyeologiya nefi i gaza*, №10, pp. 8–16.
10. Melenevsky, V., A. Kontorovich, (2007). Deep-seated (mantle) synthesis of oil: Myth or Reality?, *Tekhnologii TEK*, №1, pp.18–21.
11. Petrov, Al. A., N. N. Abruvtina, O. A. Aref'ev, et al (1994). Biomarkers and geochemical typing of crude oils. In book: *Problems of the origin of oil and gas*, Moscow, Nauka, pp. 54–87 (in Russia).
12. Rudenko, A. P. (1969). *Theory of self-development of open catalytic systems*, Moscow State University Press, 272 p (in Russia).
13. Sokolov, B. A., E. A. Abliya, (1999). *Fluids-dynamic model of oil-gas formation*, Moscow, GEOS, 79 p (in Russia).

**Bunin I.Zh., Khabarova I.A., Ryazantseva M. V., Koporulina E.V. On the change in the physical-chemical and flotation properties of sphalerite and chalcopyrite under nanosecond electromagnetic pulses**

Research Institute of Comprehensive Exploitation of Mineral Resources RAS, Moscow [bunin\\_i@mail.ru](mailto:bunin_i@mail.ru), [xabosi@mail.ru](mailto:xabosi@mail.ru)

High-voltage nanosecond pulses effectively change phase composition of a surface, electrochemical, physical-chemical and flotation properties of chalcopyrite and sphalerite: the increase of positive values of electrode mineral potential promotes the rise of anionic collector (xanthate) sorption and flotation of these minerals.

*Key words: chalcopyrite, sphalerite, nanosecond electromagnetic pulses, sorption, flotation*

**Citation:** Bunin, I.Zh, I.A.Khabarova, M.V.Ryazantseva, E.V.Koporulina (2012), On the change in the physical-chemical and flotation properties of sphalerite and chalcopyrite under nanosecond electromagnetic pulses, *Vestn. Otd. Nauk Zemle RAS*, 4, (doi: )

The effect of high-power (high-voltage) nanosecond electromagnetic pulses (HPEMP) on chemical and phase surface composition, structural-chemical, electrophysical, electrochemical, physical-chemical and flotation properties of sulphide minerals (pyrite, arsenopyrite, pyrrotite and pentlandite) has been studied in the made researches [Chanturiya et al., 2006–2008, 2011a; Chanturiya et al., 2011b; Bunin et al., 2002; Ivanova et al., 2008; Ryazantseva, 2009; Khabarova, 2011]. In this paper the new experimental data about the HPEMP effect on morphology, chemical and phase surface composition, electrochemical, sorption and flotation properties of chalcopyrite and sphalerite are presented.

**Materials and research technique.** The researches were spent on monomineral samples of chalcopyrite and sphalerite from Second Soviet deposit (Dalnegorsk ore field, Primorye Territory) with size of particles in the ranges – 100+63  $\mu\text{m}$ . The data about chemical composition and impurity contents in researched sulphide tests, received by atomic emission spectroscopy with inductive-connected plasma (ICP-AES), are presented in the table.

High-voltage nanosecond pulses treatment of minerals was made on original laboratory plant (IPKON RAS, [Chanturiya, 2006; Bunin, 2009]). The pulse duration did not exceed 10 ns, amplitude of intensity of electric component of the field strength made approximately  $\sim 10^7$  V/m, energy in a pulse was equal to 0.1 J; and pulses repetition frequency was 100 Hz; range of variation of total doze of electromagnetic pulse influence constituted the interval from 0.1 kJ to 1.5 kJ (total  $10^3$ – $1.5 \cdot 10^4$  pulses).

The morphology, sizes and elemental composition of neoformations on sulphide surfaces have been studied by analytical electron microscopy (SEM/EDX, LEO 1420 VP – INCA Oxford 350). Features of mineral surface relief on meso(nano)-scale (less than 100 nm) have been studied by scanning probe microscopy (SPM – AFM, INTEGRA Prima, NT-MDT) in semi-contact mode.

Potassium butyl xanthate (BX) sorption on mineral surface has been determined on residual concentration of collector by UV-spectrophotometry [Chanturiya and Vigdergauz, 1993] on Shimadzu UV-1700 spectrophotometer. The IR-spectra of diffuse reflection of mineral powders have been taken off in a range of wave numbers  $400 \text{ cm}^{-1}$  –  $4000 \text{ cm}^{-1}$  with the sanction  $4 \text{ cm}^{-1}$  using IR-Fourier spectrophotometer (Shimadzu, IRAffinity-1) with the diffuse reflection modulus (DRS-8000).

Electrochemical properties of minerals (electrode potential;  $E$ , mV) have been determined by method of potentiometric titration with the simultaneous control of mineral potential and pH [Chanturiya and Shafeev, 1977; Shafeev et al., 1973]. pH-value has been changed by submission of a lime solution, interval of pH was 5.5-11. Working electrodes (approximately  $10 \times 10 \times 5 \text{ mm}$ ) have been made of clean chalcopyrite and sphalerite. A comparison electrode was silver-chloride sated electrode. The dependence of electrode minerals potential from pH has been investigated previously for the raw chalcopyrite and sphalerite samples, then the minerals have been subjected to electromagnetic pulse processing and the measurements have been spent repeatedly.

**Table.** Chemical composition of chalcopyrite and sphalerite

Specimen	Cu	Fe	Zn	S	Pb	Ca	Mn	Mg	As
	Mass percent								
CuFeS <sub>2</sub>	28.54	27.54	1.91	29.17	3.19	0.70	0.044	0.01	0.006
ZnS	0.286	4.08	>50.00	29.30	6.61	0.19	0.129	0.02	0.153

Flotation activity of chalcopyrite and sphalerite has been estimated on output of a mineral in froth product, while potassium butyl xanthate (BX) (30 g/t) and methylisobutylcarbinol (MIBC) were used as reactants at pH 9.5 (CaO). Flotation experiences have been made in the laboratory flotation machine with volume 20 ml with mineral specimen 1 g with grade fineness particle – 100 +63  $\mu\text{m}$ . Interaction time with reactants was 1 minute, flotation time was 2.5 minutes. The mean square error of measurements did not exceed 5 %.

#### Transformation of structural-chemical and morphological properties of chalcopyrite and sphalerite surface under HPEMP-irradiation

Three morphological types of neoformations corresponding to the processes of structural and chemical transformations of the sulphide mineral surfaces due to the HPEMP effect (fig. 1a-c) were revealed on *chalcopyrite* surface by means of analytical electron microscopy (SEM/EDX). The first of these form dense, extended (~100  $\mu\text{m}$ ) coatings that are fractured and porous, with local swells of beadlike and irregular spherical shapes that, in some cases, decorate the breakdown channel openings (fig. 1a,b). The second phase, represented by spherical formations with sizes of 3  $\mu\text{m}$  and lower (fig. 1c), is found mainly near the breakdown regions. Superthin ( $Z \leq 100$  nm) films of the third phase, which hypothetically consist of anhydrous sulfates of copper and can be diagnosed by scanning probe microscopy (SPM-AFM, fig. 1c), uniformly cover the sulphide surface mainly in the regions where the craters and erosion holes of breakdown channels (fig. 1a) and microcracks are localized.

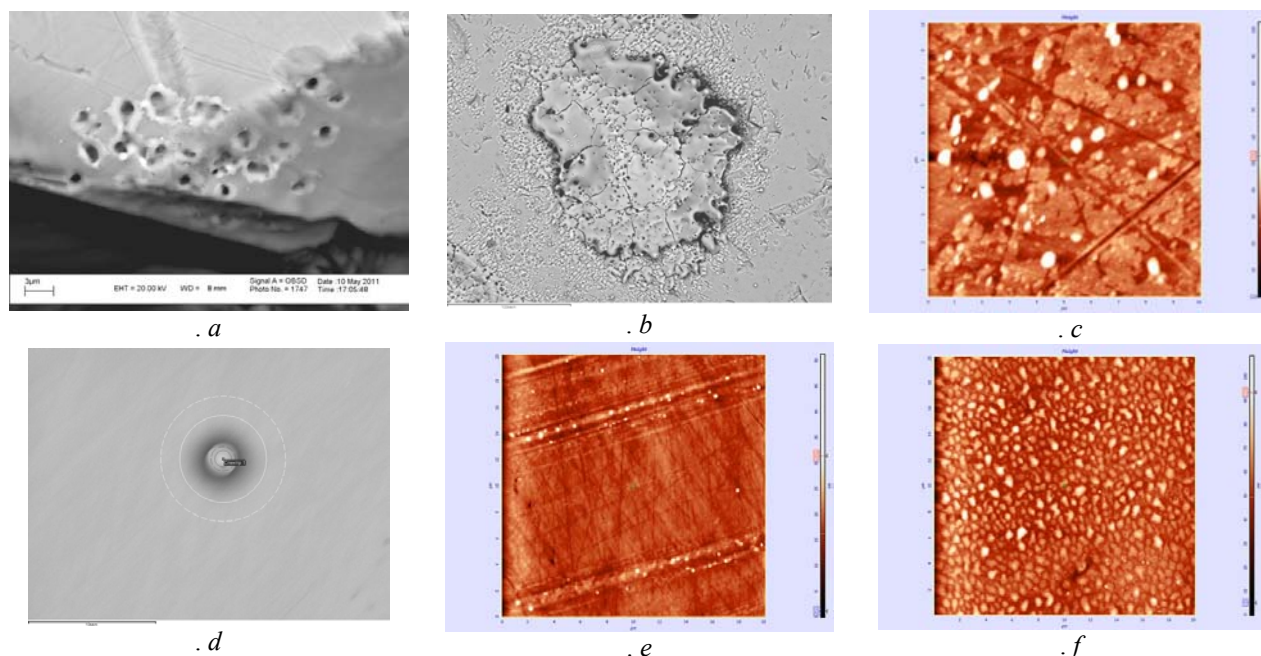


**Fig. 1.** Neoformations on chalcopyrite (a-c) and sphalerite (d-f) surface as a result of HPEMP-irradiation; SEM – EDX (a,b,d), scale bars – 2  $\mu\text{m}$  (a), 30  $\mu\text{m}$  (b), 4  $\mu\text{m}$  (d); AFM (c,e,f), scanning fields: 10x10  $\mu\text{m}$ , height Z ~ 100 nm (c); 10x10 nm, height Z ~ 40 nm (e); 10x10  $\mu\text{m}$ , height Z ~ 90 nm (f)

As against chalcopyrite, essential transformations of *sphalerite* surface morphology (fig. 1d-f) were marked only for samples subjected long electropulse treatment ( $\geq 5 \cdot 10^3$  pulses). Breakdown microchannel openings and spherical formations (with sizes of 3  $\mu\text{m}$  and lower (fig. 1d)) located along surface defects (fig. 1e) were revealed on the mineral surface. A pronounced peak corresponding to oxygen has been traced in the X-ray spectrum of a surface from these autonomous phases. With increase of duration of electropulse treatment up to approximately  $2 \cdot 10^4$  pulses, the formation of dense (such as epitaxial) layer of new structured oxide phase (fig. 1f), which hypothetically consists of copper sulfates and oxides (on the data obtained by IR-Fourier spectroscopy), was revealed on sphalerite surface.

On the results of SEM/EDX, AFM and IR-spectroscopy high-voltage nanosecond pulses in a range of

electromagnetic effect doze 0.1–1 kJ ( $10^3$ – $10^4$  pulses) result in formation and accumulation of copper sulfate  $\text{CuSO}_4$  in superficial layer of chalcopyrite, and formation and accumulation of zinc sulfate  $\text{ZnSO}_4$  and carbonate  $\text{ZnCO}_3$  on sphalerite surface. The increase of HPEMP effect intensity up to 1.5 kJ results in oxidation of sulfates and formation of copper ( $\text{Cu}_x\text{O}_y$ ) and zinc ( $\text{ZnO}$ ) oxides on sulfide surfaces. Formed micro- and nanophases are located mainly in the regions of sulfide surface heterogeneity (electrical breakdown craters, microdefects, edges and tops of crystals).

#### Effect of HPEMP on electrochemical, sorption and flotation properties of chalcopyrite and sphalerite

**Electrochemical properties.** The effect of nanosecond electromagnetic pulse processing on electrode potentials of chalcopyrite and sphalerite (fig. 2) is established. The effect of HPEMP resulted in the increase of positive

## Abstracts

values of electrode chalcopyrite potential in the mean on 25 mV at pH 6–10 (fig. 2a). In alkaline environment at pH 10–11 electrode potential  $E$  of samples processed 0.1 kJ is decreased in the mean on 20 mV; the maximal absolute difference in electrode potential values before and under HPEMP treatment ( $\Delta E = E_{pulses} - E_0$ ) equal to -

69 mV at pH 11. At increase of electropulse effect doze up to 1 kJ the maximum  $\Delta E$  equal to 43 mV at pH 11.

Electrode potential of sphalerite got more positive values at electropulse processing, being increased in the mean on 35 mV (fig. 2b). The absolute difference in values  $\Delta E$  is changed within limits of 12–70 mV, and the maximal value ( $\Delta E = 70$  mV) was got at pH 6 as a result of preliminary HPEMP processing (1 kJ).

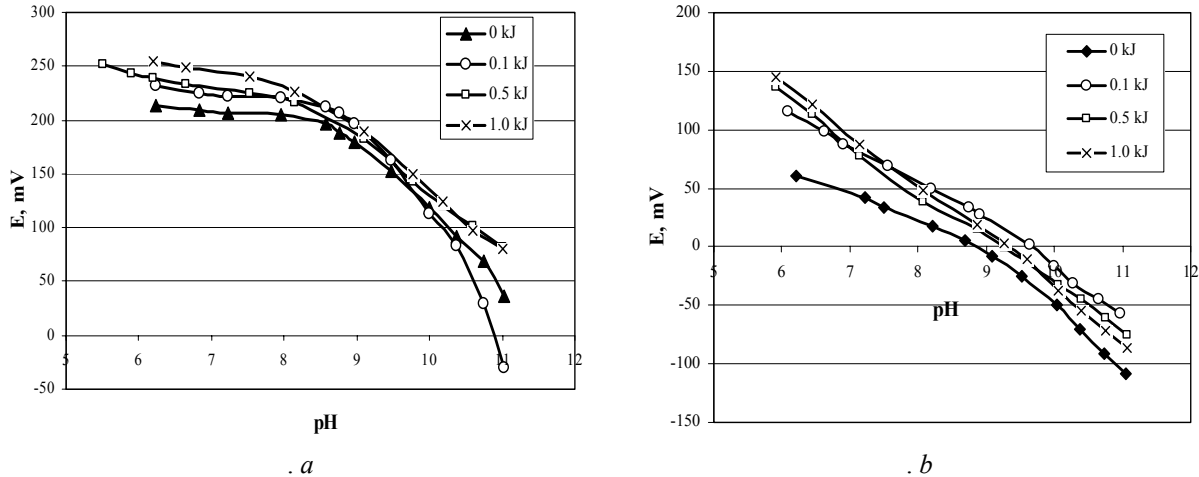


Fig. 2. Dependence of the electrode potential of chalcopyrite (a) and sphalerite (b) of pH-values before and after HPEMP-treatment

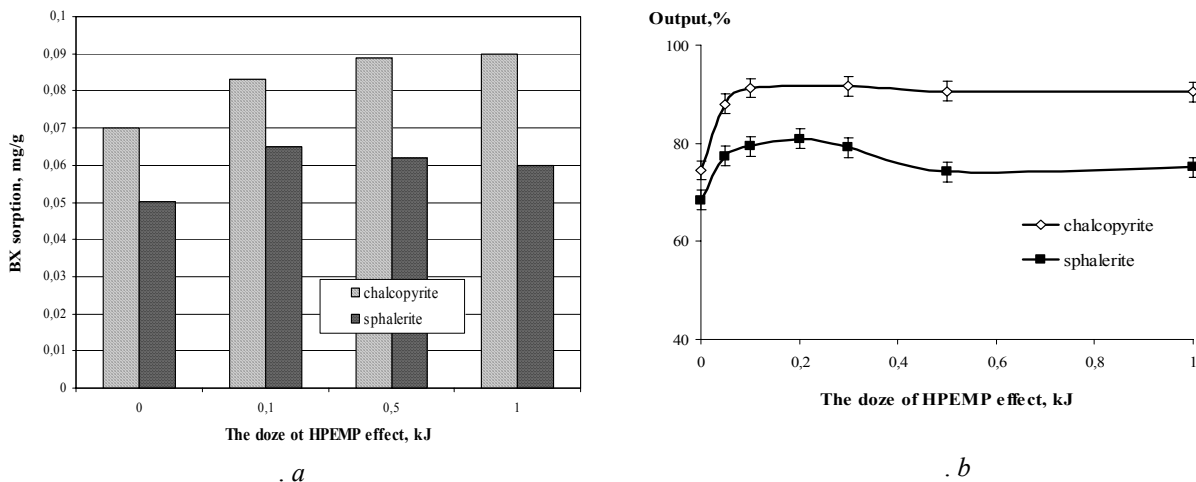


Fig. 3. Effect of HPEMP-treatment on sorption properties of chalcopyrite and sphalerite surface (pH 9.5; UV-spectrophotometry) (a) and floatability of chalcopyrite and sphalerite at pH 9.5 in the presence of BX (b)

**Sorption properties** On the UV-spectroscopy data BX sorption on chalcopyrite and sphalerite surfaces processed by HPEMP is increased (fig. 3a). Maximal BX sorption (increase at 22 %) on chalcopyrite surface is found at HPEMP effect mode  $10^4$  pulses (1 kJ). The maximum of BX sorption (increase at 23 %) on sphalerite surface is found at a mode  $10^3$  pulses (0.1 kJ). Obtained results will be coordinated to the data on electromagnetic pulse effect on electrochemical properties of sulfides: shift of electrode potentials of chalcopyrite and sphalerite in the region of positive values (fig. 2) results in increase of anionic collector sorption on minerals.

**Flotation properties** In the field of low intensity of the pulse effect (0.05–0.1 kJ), the rise of chalcopyrite floatability from 75 % to 91.5 % (fig. 3b), owing to the increase of collector amount on sulfide surface and increase of its electrode potential is established. With increase of pulse number, output of chalcopyrite in froth flotation product was not less than 90 %.

The HPEMP treatment (0.2 kJ) resulted in the increase of sphalerite floatability from 69 % (without preliminary pulse processing) to 81.5 % is observed (fig. 3b). The maximal output of the mineral in froth flotation product (increase on 10–12 %) was got at 0.05–0.3 kJ (fig. 3b). This fact is caused by the increase of BX amount on sphalerite surface and shift of electrode potential in the region of positive values. With increase of power effect doze the decrease of mineral output in froth product up to 74 % (0.5 kJ) and 76 % (0.1 kJ) is established.

Thus, on the basis of these experimental data about mechanisms of structural-chemical transformations of chalcopyrite and sphalerite surfaces at the effect of high intensity fields, it is possible to make a conclusion about an opportunity of high-voltage nanosecond pulses application for development of innovation technologies, which directionally modified physical-chemical and technological properties of sulphide minerals.

### Conclusion

1. As a result of made spectroscopical researches of high-voltage nanosecond pulses effect on phase composition of chalcopyrite and sphalerite surfaces, the range of change of electromagnet pulse influence doze is established and equal to 0.1–1 kJ ( $10^3$ – $10^4$  pulses). At which there is the formation and accumulation of copper sulfate  $\text{CuSO}_4$  in superficial layer of chalcopyrite, and zinc sulfate  $\text{ZnSO}_4$  and carbonate  $\text{ZnCO}_3$  on sphalerite surface. The increase of HPEMP effect intensity up to 1.5 kJ results in oxidation of sulfates and formation of copper ( $\text{Cu}_x\text{O}_y$ ) and zinc ( $\text{ZnO}$ ) oxides on sulphide surfaces.

2. The experimental data showing of the change of electrochemical chalcopyrite and sphalerite properties owing to preliminary electromagnetic pulse treatment of minerals, namely, increase of positive values of electrode sulfide potential are received. It is promotes increase of anionic collector (xanthate) sorption and flotation of these minerals.

3. For monomineral flotation of chalcopyrite and sphalerite, optimal conditions (range of the HPEMP doze change was from 0.05 kJ to 0.3 kJ) for preliminary electromagnetic pulse processing of sulphides is established and experimentally proved. At which it is essential (in the mean on 10–15 %) raises mineral flotation.

*The authors acknowledge the financial supports from the RFJBR (Grant no 11-05-00434-a) and the Program of the Scientific School of Russian Federation (Grant no NSh-220.2012.5) and the Grant from the President of the Russian Federation (Grant no MK-1968.2012.5).*

### References:

- Bunin, I. Zh., T. A. Ivanova, V. D. Lunin (2002). Effect of high-energy impacts on the process of dissolution of gold-containing minerals, *Mining Informational and Analytical Bulletin (Scientific and Technical Journal)*, №8, pp.172–176.
- Bunin, I. Zh. (2009). Theory of nanosecond electromagnetic pulses effect on disintegration and breaking-up process of fine-disseminated mineral complexes and noble metals recovery from ores, *Synopsis of Grand PhD thesis*, Moscow, MGRI-RSGPU, 39 p.
- Chanturiya, V.A., R. Sh. Shafeev (1977), *Chemistry of surface phenomena in flotation*, Moscow, Entrails, 191 p.
- Chanturiya, V. A., V. E. Vigdergauz (1993). *Electrochemistry of sulphides. Theory and practice of flotation*, Moscow, Nauka, 206 p.
- Chanturiya, V. A., K. N. Trubetskoi, S. D. Victorov, I. Zh. Bunin (2006). *Nanoparticles in processes for disintegration and breaking-up of geomaterials*, Moscow, ICEMR RAS (IPKON RAN), 216 p.
- Chanturiya, V. A., T. A. Ivanova, I. A. Khabarova, M. V. Ryazantseva (2007). Effect of ozone on physico-chemical and flotation properties of surface of pyrrhotite under the nanosecond electromagnetic pulses treatment, *Journal of Mining Science*, v.43, №1, pp.83–90.
- Chanturiya, V. A., I. V. Filippov, L. O. Filippov, M. V. Ryazantseva, I. Zh. Bunin (2008). Effect of powerful electromagnetic impulses on surface and flotation properties of carbonate-bearing pyrite and arsenopyrite, *Journal of Mining Science*, v.44, №5, pp.518–530.
- Chanturiya, V. A., I. Zh. Bunin, M. V. Ryazantseva, I. V. Filippova, E. V. Koporulina (2011a). Nanosecond electromagnetic pulse effect on phase composition of pyrite and arsenopyrite surface, their sorption and flotation properties, *Journal of Mining Science*, v.47, №4, pp.506–513.
- Chanturiya, V. A., I. Zh. Bunin, M. V. Ryazantseva, L. O. Filippov (2011b). Theory and application of high-power

nanosecond pulses to processing of mineral complexes, *Mineral Processing and Extractive Metallurgy Review*, vol.32, №2, pp. 105–136.

- Ivanova, T. A., I. Zh. Bunin, I. A. Khabarova (2008). On the characteristic properties of oxidation of sulfide minerals exposed to nanosecond electromagnetic pulses, *Bulletin of the Russian Academy of Sciences: Physics*, v. 72, №10, pp.1326–1329.
- Khabarova, I. A. (2011). Increase of physics-chemical and flotation contrast properties of pyrrhotite and pentlandite using high-power electromagnetic pulses, *Synopsis of Ph.D thesis*, Moscow, ICEMR RAS (IPKON RAN), 22 p.
- Ryazantseva, M. V. (2009). Mechanism of nanosecond electromagnetic pulses effect on structural-chemical and flotation properties of pyrite and arsenopyrite, *Synopsis of Ph.D thesis*, Moscow, ICEMR RAS (IPKON RAN), 19 p.
- Shafeev, R. Sh., V. A. Chanturiya, V. P. Yakushkin (1973). *Effect of ionization radiation on flotation process*, Moscow, Nauka, 58 p.

### Gribov S. K., Dolotov A. V. Experimental study of kinetics of isothermal dehydroxylation of natural goethite

Borok Geophysical Observatory – the branch of Foundation of the Russian Academy of Sciences Schmidt Institute of Physics of the Earth RAS, Yaroslavl distr [gribov@borok.yar.ru](mailto:gribov@borok.yar.ru); [adolotov@borok.yar.ru](mailto:adolotov@borok.yar.ru)

Changes of saturation magnetization on time during the process of isothermal dehydroxylation of natural goethite are studied. The activation energy of the phase transition goethite  $\rightarrow$  hematite was determined and the estimation of structural stability of investigated goethite fraction in the earth's surface was also carried out.

**Key words:** goethite, hematite, isothermal kinetics, saturation magnetization

**Citation:** Gribov, S. K., A. V. Dolotov (2012), Experimental study of kinetics of isothermal dehydroxylation of natural goethite, *Vestnik ONZ RAS*, 4, (doi: )

The reaction of goethite dehydroxylation  $\alpha\text{-FeOOH}\cdot n\text{H}_2\text{O} \rightarrow \alpha\text{-Fe}_2\text{O}_3 + n\text{H}_2\text{O}$  is the most common process of hematite ( $\alpha\text{-Fe}_2\text{O}_3$ ) formation in sedimentary rocks. However, kinetic studies of this phase transition are still not enough to answer the questions of how long this process is extended in time under natural conditions and how great mineralogical stability of goethite is. Meanwhile, it is very important to know in order to assess the possibility of formation and preservation of both primary and secondary chemical magnetization (CRM), especially in red sedimentary formations during diagenesis.

In this work a kinetic study was carried out on natural goethite fraction, which was a dense powder aggregates consisting of needle-shaped particles (with an average size of 400x50 nm), elongated along the crystallographic *c*-axis of goethite. According to the results of X-ray powder diffraction (XRPD) analysis, the original fraction was described by the orthorhombic (space group *Pbnm*, *Z* = 4) unit cell with *a* = 4.6095 Å, *b* = 9.9699 Å, *c* = 3.0250 Å and volume *V* = 139.02 Å<sup>3</sup>, in close agreement with standard values (ICDD PDF-2 Release 2008 database, card 00-029-0713). Average crystallite sizes *L* (or more exactly the regions of coherent X-ray scattering along the normal to reflecting (*hkl*) planes calculated from the broadening of the diffraction peaks) for primary goethite were ~ 34.8 nm, ~ 50.6 nm and > 70 nm along the [100], [010] and [001]

## Abstracts

directions, respectively, which is consistent with a needle-like morphology.

The study of transformation of the primary goethite fraction by dynamic thermogravimetry (TG) (a constant heating rate of  $\nu = 10\text{ }^{\circ}\text{C}/\text{min}$  from room temperature till  $1000\text{ }^{\circ}\text{C}$  in air) showed  $\sim 0.49\%$  of weight loss of starting material by heating to  $150\text{ }^{\circ}\text{C}$  (corresponding to the loss of the chemisorbed surface water) and decrease  $\sim 9.62\%$  of weight between  $240$  and  $370\text{ }^{\circ}\text{C}$  (due to the removal of structural hydroxyls (OH) and corresponding to the endothermic transformation from the goethite elementary lattice to the hematite one). Further heating up to  $1000\text{ }^{\circ}\text{C}$  yielded an additional  $\sim 0.96\%$  of weight loss. Thus, non-isothermal TG analysis showed a total amount of weight loss after the phase transformation in air was a bit larger than the theoretical expectation ( $10.1\%$ ) for stoichiometric goethite. Based on these results, the formula of the starting goethite can be written in the form of  $\text{FeOOH} \cdot 0.0538\text{H}_2\text{O}$ . According to thermomagnetic (by saturation magnetization  $J_S$ ) analysis ( $\nu = 4\text{ }^{\circ}\text{C}/\text{sec}$ ) of initial samples, the Neel temperature ( $T_N$ ) of goethite fraction was  $\sim 120\text{ }^{\circ}\text{C}$ , the temperature range of the phase transition goethite $\rightarrow$ hematite was ( $250 - 380$ )  $^{\circ}\text{C}$ , the Curie temperature ( $T_C$ ) of formed hematite was  $\sim 673\text{ }^{\circ}\text{C}$ . According to XRPD data final hematite phase was characterized by the following parameters (after goethite decomposition at  $250\text{ }^{\circ}\text{C}$  for 312 hours):  $a = 5.036\text{ \AA}$ ,  $c = 13.753\text{ \AA}$ ,  $V = 302.1\text{ \AA}^3$  in the hexagonal setting  $R\bar{3}C$  at  $L > 60\text{ nm}$  in crystallographic direction  $[110]$ , which coincided with the texture axis of  $\alpha\text{-Fe}_2\text{O}_3$  particles.

In the present study the kinetics of dehydroxylation of  $\alpha\text{-FeOOH}$  into  $\alpha\text{-Fe}_2\text{O}_3$  was investigated in air under isothermal conditions using a magnetometer method by *in situ* measuring the change in saturation magnetization ( $J_S$ ) for 312 hours in a constant magnetic field of 0.65 Tesla during heating at one of 11 temperatures between  $183\text{ }^{\circ}\text{C}$  and  $273\text{ }^{\circ}\text{C}$ . The first relatively low temperature corresponding to the beginning of the process of dehydroxylation was chosen in order to bring your laboratory experiments to real environmental conditions, but still be able to conduct them on selected laboratory time scale; the highest temperature of isothermal heating, according to the results of TG analysis of fresh samples, corresponded to the interval of maximum reaction rate.

The isothermal dependences of the change of saturation magnetization on the time of induced dehydroxylation of original goethite fraction are depicted in Fig. 1. In the kinetic curves  $J_S(t)$  behavior can be traced the following regularities: marked decrease of  $J_S$  at an initial period of time (A segment), than follows a period of change in the falling slope; herewith, in the temperature range ( $198 - 273$ )  $^{\circ}\text{C}$ , one or two (B and C respectively) segments of exponential decrease of saturation magnetization, the locations of which vary with temperature, are shown on the  $J_S(t)$  curve. Moreover, the slope of C segment of the  $J_S(t)$  curve is always the steepest than in the previous segments. It is also significant that the kinetic curves of the  $J_S(t)$ , recorded during the decomposition of goethite fraction during 312 hours at  $T \geq 204\text{ }^{\circ}\text{C}$ , show a little different and stable (within the measurement accuracy) values of  $J_S$  at the final stages of

the  $J_S(t)$  measurements (D segment), covering the most significant period of time at this reaction stage (Fig. 1). It is also important to note that as a result of the isothermal dehydroxylation of goethite the maximum drop in saturation magnetization was  $\sim 2$  times.

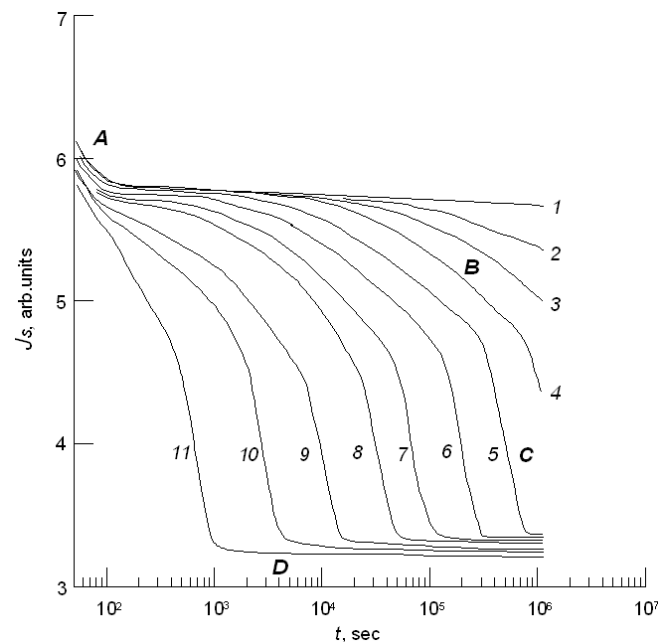


**Fig. 1.** Changes in saturation magnetization as a function of time (logarithmic scale) and the temperature of dehydroxylation of the initial goethite fraction. The numbers 1–11 marked curves corresponding to different reaction temperatures: 1 –  $183\text{ }^{\circ}\text{C}$ , 2 –  $187\text{ }^{\circ}\text{C}$ , 3 –  $191\text{ }^{\circ}\text{C}$ , 4 –  $198\text{ }^{\circ}\text{C}$ , 5 –  $204\text{ }^{\circ}\text{C}$ , 6 –  $210\text{ }^{\circ}\text{C}$ , 7 –  $216\text{ }^{\circ}\text{C}$ , 8 –  $223\text{ }^{\circ}\text{C}$ , 9 –  $235\text{ }^{\circ}\text{C}$ , 10 –  $248\text{ }^{\circ}\text{C}$ , 11 –  $273\text{ }^{\circ}\text{C}$ . A, B, C and D are characteristic segments of the curves discussed in the text.

According to thermomagnetic analysis of annealed samples (Fig. 2) it was found that the dehydroxylation of goethite during 312 hours at  $T = 183\text{--}198\text{ }^{\circ}\text{C}$  leads to the coexistence of goethite and hematite phases. Moreover, it was found that in the course of the reaction (with a temperature increase)  $T_n$  of the residual goethite steadily increases from  $120$  to  $191\text{ }^{\circ}\text{C}$ , the maximum phase transition temperature decreases from  $380\text{ }^{\circ}\text{C}$  to  $367\text{ }^{\circ}\text{C}$ , whereas  $T_C$  of the hematite components is  $\sim 668\text{--}671\text{ }^{\circ}\text{C}$ . Herewith, the observed increase of the  $J_S(T)$  of hematite component, probably dues to the Hopkinson effect – increasing of the weak ferromagnetic moment of the hard magnetic material in an external magnetic field which is small compared with the saturation fields. The samples, which were dehydroxylated during the same time period at  $T \geq 204\text{ }^{\circ}\text{C}$ , are always of single phase with  $T_C \sim 673\text{ }^{\circ}\text{C}$  (Fig. 2).

On the basis of X-ray diffraction studies of the samples subjected to prolonged isothermal dehydroxylation [Gribov and Dolotov, 2011] and analysis of published data we can make the following preliminary conclusions. The initial (A) section of the kinetic  $J_S(t, T)$  curve (Fig. 1) is obviously the result of the manifestation of weak ferromagnetism of starting goethite with  $T > T_n$ . Recession  $J_S(t)$  for arbitrarily selected A and B sections corresponds to dehydroxylation, which leads to the hematite formation on the surface of goethite grains and within them, respectively. Completion of the recession

$J_s(t)$  ( $D$  section of this curve) corresponds to a complete phase transformation at the reaction temperature indicated on the graph.

For selected ( $B$  and  $C$ ) sections of predominantly exponential reduction in the magnetization of the kinetic  $J_s(t)$  curves, the values of the effective activation energy ( $E$ ) of hematite formation from goethite, calculated from the linear dependence of experimentally obtained  $\ln(dJ_s/dt)$  vs.  $1/T$  within the temperature range of 204–273 °C, were equal and made up  $\sim 201.48$  kJ/mol. This fact indicates that the rate-limiting step of the process of goethite dehydroxylation is the diffusion of  $\text{Fe}^{3+}$  cations. It should be also noted that this  $E$  value is in a good agreement with that obtained from the thermogravimetric method in a similar decomposition temperature range of original samples [Gribov and Dolotov, unpublished manuscript, 2012]. For comparison, the values of the activation energies of goethite dehydroxylation according to literature data are in the range of 88 – 247 kJ/mol, and are largely dependent on the size of the goethite particles [Cornell and Schwertmann, 2003].

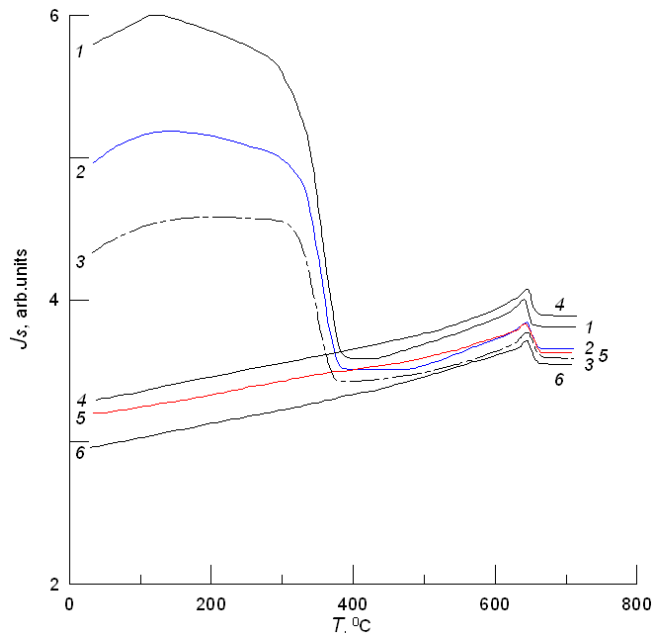


**Fig. 2.** Thermal demagnetization curves of saturation magnetization for samples dehydrated during 312 hours at different temperatures: 1 – 183 °C, 2 – 191 °C, 3 – 198 °C, 4 – 210 °C, 5 – 223 °C, 6 – 273 °C.

The temporal extrapolation of the magnetometric kinetic curves to the  $J_s$  values, corresponding to the total transformation of goethite into hematite, allowed to estimate the time  $t^*$ , required to complete the phase transition in the investigated temperature range (204 to 273 °C). The linearity of the obtained dependence  $\ln t^*$  vs.  $1/T$  (Fig. 3) gives the possibility of its extrapolation to lower temperatures, i.e. allows us to enter the times that are not available for laboratory researches. As occurred, in natural conditions the total spontaneous transformation of investigated goethite fractions can be implemented for the period of  $\sim 1$  or  $\sim 10$  million years only in the case of a regional heating of the rock to temperatures of  $\sim 85$  and  $\sim 73$  °C, respectively. These estimates give a reason to believe that in the earth's surface in goethite-bearing sedimentary rocks the formation of hematite with attendant CRM components does not occur during or

immediately after deposition but rather it is occurred over a long period of time enough to span one or more geomagnetic polarity reversal. In such cases, the spontaneous dehydroxylation of goethite to hematite may play a definite role in the chemical remagnetization of red sedimentary formations in the hypergenesis zone.

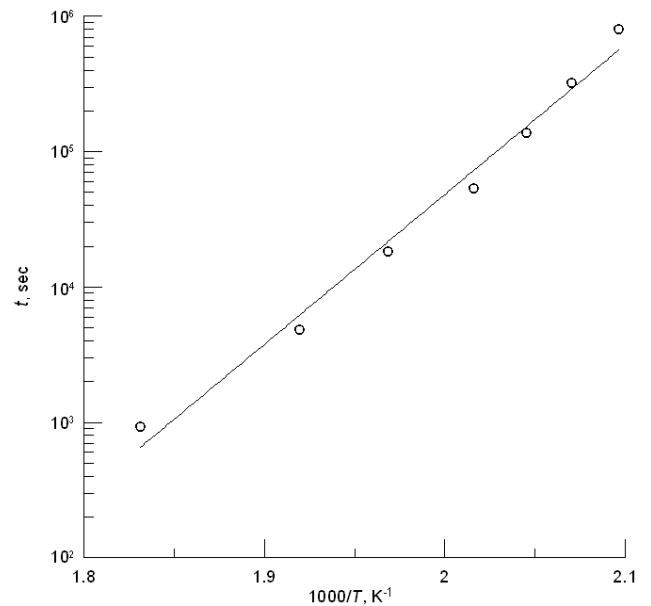


**Fig. 3.** The dependence of the calculated time (logarithmic scale) of complete hematization of the original goethite fraction against inverse Kelvin temperature ( $1/T$ ). The solid line drawn on the graph is the best linear fit to the data points.

The work has been supported by RFBR (grant 09-05-00471).

#### References:

- Gribov, S. K., A. V. Dolotov (2011). Peculiarities of isothermal dehydration of natural goethite ( $\alpha\text{-FeOOH}$ ): a X-ray diffraction study, «Physical-chemical and petrophysical researches in the Earth's sciences», *Proceedings of the twelve conference*, Moscow, pp. 89–92.
- Cornell, R. M., U. Schwertmann (2003). The iron oxides: structure, properties, reactions, occurrences and uses, 2<sup>nd</sup> ed. Wiley-VCH, p. 664.

#### Khodakovskiy I.L. About a new semi-empirical equations of temperature dependence of heat capacity and thermal expansion coefficient of solids

Dubna University, Chemistry, Geochemistry and Cosmochemistry Department, Universitetskaya Str. 19, Dubna, Moscow Region, Russia [igor-kho@yandex.ru](mailto:igor-kho@yandex.ru)

The empirically established polynomial form of the  $C_p$  equations for solids at  $T > 298.15$  K recommended by Maier and Kelley (1932), Haas and Fisher (1976), Berman and Brown (1985), as a rule, can be used for the data interpolation. In 1986 Fei and Saxena, and, independently, Khodakovskiy, are proposed semi-empirical equations, using well known  $C_V$  approaches to  $3Rn$  constant value (where  $R$  is the gas constant, and  $n$  is a number of atoms) at  $T \rightarrow \infty$ , and thermodynamic relation  $C_p - C_V = \alpha^2 V K_T T$  as well. However, their forms  $C_p$  equations approach to  $\infty$  (not to zero) at  $T \rightarrow 0$ .

The equation (1):  $C_p = a[1 - 1/(1 + cT^2)] + bT$  was proposed by Kuznetsov and Kozlov (1988). This new type

## Abstracts

equation, unlike previous ones, corresponds to third law of thermodynamic ( $C_p = 0$  at  $T = 0$ ), but does not obey the «Debye  $T^3$  law» at low temperatures (*i.e.* the temperature dependence is not expressed in terms of  $AT^3$  where  $A$  is a constant). The equation (2):  $C_p = Rn\{[a_3T^3/(1 + a_3T^3)] + [b_2T^2/(1 + b_2T)] + [c_1T/(1 + c_1T)]\} + \alpha^2VK_T T$  was proposed by Khodakovskiy in 2000. The equation (2) are examined using the  $C_p$  experimental data for different types of solids. In this paper, as a result of preliminary investigations, it is found that the last term of an equation (2) should be excluded, but a new adjusting parameter  $k$  should be included:

$C_v = Rn[kL_D + (3 - k)L_E]$ , where  $L_D = [1 - 1/(1 + bT^3)]$  and  $L_E = [1 - 1/(1 + bT^2)]$

The empirically established form of the  $\alpha$  equations recommended by different authors can be used for the data interpolation only. Because the ratio  $C_p/\alpha \approx \text{const}$ , the following equations:  $\alpha = a [1 - 1/(1 + bT^2)]$  may be good for representation, estimation, and high (low) temperature extrapolation of  $\alpha$ . In this case the thermodynamic limitations:  $\alpha = 0$ , and  $C_p - C_v = \alpha^2VK_T T = 0$  at  $T = 0$  will be obeyed exactly.

### Kokh M. A., Tagirov B. R., Kovalchuk E. V. Formation of gold-bearing sulfides of copper in connection with a problem of «invisible gold»: experimental study

The Institute of Geology of Ore Deposits, Petrography, Mineralogy, and Geochemistry RAS, Moscow [kokhmaria@mail.ru](mailto:kokhmaria@mail.ru), [tagir@igem.ru](mailto:tagir@igem.ru)

In the system saturated with the metal gold, copper sulfides (covellite  $\text{CuS}$ , digenite  $\text{Cu}_{9+x}\text{S}_5$ , and chalcocite  $\text{Cu}_2\text{S}$ ) were obtained by the method of hydrothermal synthesis. It is established that under conditions of experiments (450°C, 700–1150 bar) the contents of «invisible» (isomorphous or submicron) gold in digenite and chalcocite are lower than the limit of detection of X-ray spectral microanalysis (<0.008 wt.%). Covellite, on the other hand, can contain to 0.3 wt. % of gold evenly distributed over the volume of the solid phase. The content of gold in covellite increases as the sulfur volatility grows.

**Key words:** hydrothermal processes, sulfides, experiment, chalcocite, digenite, covellite, gold, isomorphism.

**Reference:** Kokh, M. A., B. R. Tagirov, E. V. Kovalchuk (2012). Formation of gold-bearing sulfides of copper in connection with a problem of «invisible gold»: experimental study, *Vestnik ONZ RAS*, 4, (doi: )

### Kotelnikov<sup>1</sup> A.R., Ananiev<sup>2</sup> V.V., Suk<sup>1</sup> N.I., Akhmedjanova<sup>1</sup> G.M. Synthesis of phosphorus- and arsenic-bearing feldspars

<sup>1</sup>Institute of Experimental Mineralogy RAS, Chernogolovka [kotelnik@iem.ac.ru](mailto:kotelnik@iem.ac.ru)

<sup>2</sup>Institute of Volcanology and Seismology FEB RAS

The synthesis of phosphorus- and arsenic-bearing sodium (potassium) feldspars have been carried out in hydrothermal conditions at  $T=400\div 600^\circ\text{C}$ ,  $P=1.5$  kbar. The microprobe analysis of synthetic P-, As- bearing feldspars was carried out. Cell parameters were calculated from X-ray data. It is shown a good correlation between cell parameters of different feldspars and average means of radius of tetrahedral cations.

**Key words:** synthesis, feldspars, cell parameters, solid solutions

**Citation:** Kotelnikov, A. R. , V. V. Ananiev, N. I. Suk, G. M. Akhmedjanova (2012), Synthesis of phosphorus- and arsenic-bearing feldspars, *Vestn. Otd. nauk Zemle*, 4,

### Kotelnikov A. R., Kovalsky A. V., Suk N. I. The study of Mg and Fe distribution between ternary solid solutions of clinopyroxenes and biotite

Institute of Experimental Mineralogy RAS, Chernogolovka [kotelnik@iem.ac.ru](mailto:kotelnik@iem.ac.ru)

Ternary solid solutions of alkaline clinopyroxenes (CPx3) with constant content of aegirine minal (20 mol.%) were synthesized. Based on the x-ray study the cell parameters refinement has been produced. The ternary solid solutions are characterized by alternating deviation from ideality. The cation exchange runs between CPx3 and biotite were carried out at 750°C and 1.5 kbar under hydrothermal conditions. The isotherm of Mg,Fe distribution between clinopyroxene and biotite was obtained. The distribution coefficient of Mg between clinopyroxene and biotite ( $K_D$ ) is described by following 3-order equation:  $\ln(K_D) = 0.65 + 3.30*x - 5.763*x^2 - 1.0911*x^3$ ; where  $x=(\text{Mg}/(\text{Mg}+\text{Fe}^{2+}))$  in clinopyroxene. The calculation of excess free energy of mixing of clinopyroxene was carried out based on experimental data.

**Key words:** solid solutions, clinopyroxene, biotite, cell parameters, coefficient of element distribution

**Citation:** Kotelnikov A. R. , A. V. Kovalsky, N. I. Suk (2012), The study of Mg and Fe distribution between ternary solid solutions of clinopyroxenes and biotite, *Vestn. Otd. nauk Zemle*, 4,

### Kovalchuk<sup>1</sup> E. V., Chareev<sup>2</sup> D. A., Tagirov<sup>1</sup> B. R., Kokh<sup>1</sup> M.A., Mokhov<sup>1</sup> A. V. Breakdown structures of synthetic solid solutions in the system Cu–Fe–Au–S

<sup>1</sup>Institute of geology of ore deposits RAS

<sup>2</sup>Institute of Experimental Mineralogy RAS [geofishko@gmail.com](mailto:geofishko@gmail.com)

The sulfides of Cu and Fe were synthesized using salt-flux method at 650–700 °C in the presence of excess Au. The following sulfides were found in the products of the experiments: i) phases whose composition falls within the bornite field ( $\text{Cu}_2\text{S}-\text{Cu}_5\text{FeS}_4$ ), ii) chalcocopyrite ( $\text{CuFeS}_2$ ), iii) sulfides with composition close to nukundamite ( $\text{Cu}_{3.4}\text{FeS}_4$ ), idaite ( $\text{Cu}_{5.5}\text{FeS}_{6.5}$ ), and covellite ( $\text{CuS}$ ). In bornite Au exists as a phase that forms lamellae that are typical for decomposition (substitution) structures, but in nukundamite (idaite) it forms segregations of copper gold or a phase with composition close to  $\text{CuAuS}$ . In the run products this phase exists in the form of small homogeneous “fresh” grains, or forms heterogeneous “worm-like” aggregates.

**Key words:** sulfides, bornite, chalcocopyrite, gold, synthesis, salt-flux

**Citation:** Kovalchuk, E. V., D. A. Chareev, B. R. Tagirov, M. A. Kokh, A. V. Mokhov. (2012), Breakdown structures of synthetic solid solutions in the system Cu–Fe–Au–S e, *Vestn. Otd. nauk Zemle*, 4,

### Kravchenko<sup>1</sup> T.A., Nenasheva S.N.<sup>2</sup> Experimental study of phase compositions in the region of chalcopyrite solid solution crystallization

<sup>1</sup>Institute of geology and mineralogy SB RAS, [tanyuk@igm.nsc.ru](mailto:tanyuk@igm.nsc.ru).

<sup>2</sup>Petersburg Mineral Museum RAS

Compositions of chalcopyrite solid solution crystallization products have been studied to determine characteristics of formation of phase equilibria with chalcopyrite  $\text{CuFeS}_2$ , cubanite  $\text{CuFe}_2\text{S}_3$ , talnakhite  $\text{Cu}_9\text{Fe}_8\text{S}_{16}$ , mooihokite  $\text{Cu}_9\text{Fe}_9\text{S}_{16}$  and haycockite  $\text{Cu}_4\text{Fe}_5\text{S}_8$  in the process of the Cu-Fe sulfide melt crystallization. The determined Cu/Fe relations of tetragonal chalcopyrite (1.03–0.67), cubic fcc cubanite (0.61–0.39) and cubic pc haycockite

(0.92–0.68) considerably differ from correspondent formula relations. Composition of mooihoeikite with Cu/Fe = 1.04–0.93 corresponds to the bornite – mooihoeikite - cubanite equilibrium line, which crosses chalcopyrite and haycockite phase associations regions.

**Key words:** Cu-Fe-S system, chalcopyrite solid solution, crystallization of the melt

**Reference:** Kravchenko, T. A., S. N. Nenasheva (2012), Experimental study of the phase compositions in the field of the chalcopyrite solid solution crystallization, *Vestnik ONZ RAS*, 4,

In respect of the composition the following minerals refer to the region of chalcopyrite solid solution crystallization: chalcopyrite CuFeS<sub>2</sub>, talnakhite Cu<sub>9</sub>Fe<sub>8</sub>S<sub>16</sub>, cubanite CuFe<sub>2</sub>S<sub>3</sub>, mooihoeikite Cu<sub>9</sub>Fe<sub>9</sub>S<sub>16</sub> and haycockite Cu<sub>4</sub>Fe<sub>5</sub>S<sub>8</sub>. All of them are characterized by variable compositions but the limits of their compositions variation have not been established. This complicates determination of phase equilibrium formation characteristics during the Cu-Fe sulfide melt crystallization. Whereas in the given study the results of various experiments on the synthesis of phase associations of central part of the Cu-Fe-S system: 45–50 at.% S, Cu/Fe = 1.44–0.25 have been further studied and generalized [Kravchenko, Nigmatulina, 2009; Kravchenko, 2009, 2011]. The obtained results allowed to specify the compositions of synthesized chalcopyrite solid solution crystallization products and to supplement the phase relations scheme [Kravchenko, 2011] with talnakhite – mooihoeikite and mooihoeikite – haycockite equilibria lines (Fig.). The synthesis has been carried out in the evacuated quartz ampoules by cooling the melt from 1150–1100 °C to room temperature and its further annealing at 800, 600 and 400 °C. The synthesized samples have been studied using optical microscope, X-ray diffraction and microprobe analysis methods.

The results are shown in the figure and in table 1 below. The determined Cu/Fe relations of synthesized tetragonal chalcopyrite, isocubanite (cubic fcc cubanite), talnakhite, mooihoeikite and cubic pc haycockite differ from the correspondent formula relations. The association isocubanite + pyrrhotite Fe<sub>1-x</sub>S (cb + po) with the same isocubanite composition as in the association isocubanite + haycockite + pyrrhotite (cb + hc + po) but with more sulfur pyrrhotite, and the association chalcopyrite +

isocubanite + pyrrhotite (cp + cb + po) with stoichiometric isocubanite and chalcopyrite and enriched by sulfur pyrrhotite are not shown in the table 1.

**Isocubanite, chalcopyrite, talnakhite.** Isocubanite has been established in associations with all synthesized chalcopyrite solid solution crystallization products. The most high-melting isocubanite has been crystallized from melt the first, and its composition determines compositions of the equilibrium phases. The copper-enriched isocubanite (Cu/Fe = 0.61–0.52) is crystallized in associations with chalcopyrite or talnakhite depending on the cooling regime of the melt in interval of 1000–800 °C. By cooling melt with keeping at 850 °C isocubanite is crystallized with chalcopyrite (Cu/Fe = 0.99–0.67), whereas without keeping at 850 °C — with talnakhite (Cu/Fe = 1.16–1.09) and less iron-enriched but more copper-enriched chalcopyrite (Cu/Fe = 1.03–0.92). In case of the quick cooling of melt with Cu/Fe = 1–0.67 from 850 °C to room temperature in chalcopyrites with Cu/Fe = 0.99–0.82: 25–22.5 at.% Cu, 25–27.5 at.% Fe, the regions of exsolution textures with phase composition of maximal iron-enriched chalcopyrite (Cu/Fe = 0.67: 20 at.% Cu, 30 at.% Fe) are found. Thereby Cu/Fe of chalcopyrite is changed within 1.03–0.67. As the cooling melt speed increases and the sulfur composition decreases the region of iron-enriched chalcopyrite crystallization decreases.

The phase relations typical for the exsolution textures of solid solution have been determined for chalcopyrite – containing phase associations only. The phase compositions and X-ray diffraction pictures of mixtures of chalcopyrite with talnakhite and isocubanite indicate that the studied exsolution textures talnakhite + chalcopyrite and isocubanite + chalcopyrite are caused by phase transition of cubic fcc iss to tetragonal chalcopyrite. The obtained results confirm the experimental data [Yund, Kullerud, 1966; Sugaki et. all, 1975 etc.] demonstrating variability of chalcopyrite composition. Composition of maximal iron-enriched chalcopyrite synthesized in the given study corresponds to composition of maximal iron-enriched iss determined [Tsumura and Kitakaze, 2004] in the 50 at.% S section of Cu-Fe-S system at 800 °C.

**Table 1.** Composition of synthesized phases

Phase association	Phases	Composition of phases, at. %			Cu/Fe
		Cu	Fe	S	
cb + cp	cb	17.34–19.32	31.75–33.13	48.93–49.53	0.61–0.52
		23.92–26.78	38.70–40.17	34.22–34.46	
	cp	20.31–25.54	25.81–30.47	48.65–49.81	0.99–0.67
		28.03–34.97	31.07–36.96	34.37–34.48	
cb + tal + cp tal + cp + bn cp + bn + py	cp	24.22–25.43	24.71–26.42	49.36–49.86	1.03–0.92
		33.40–34.86	29.76–32.02	34.34–34.48	
	tal	26.92–27.92	24.12–24.60	47.75–48.84	1.16–1.09
		36.64–37.68	28.75–29.13	32.74–33.42	
mh + bn	mh	25.64–27.38	26.37–27.52	46.25–47.15	1.04–0.93
		34.74–37.18	31.46–32.83	31.68–32.25	
po + cb+ hc	cb	14.04–16.80	34.06–35.90	49.13–50.06	0.49–0.39
		19.59–23.34	41.57–44.03	34.42–35.25	
	hc	21.01–25.35	28.17–31.05	45.97–47.94	0.90–0.68
		30.65–34.34	33.74–36.17	31.43–32.91	
po + hc + bn	hc	21.61–25.75	27.91–31.98	46.41–47.25	0.92–0.68
		29.46–34.71	33.06–38.32	31.93–32.74	

cb — isocubanite CuFe<sub>2</sub>S<sub>3</sub> (Cu/Fe = 0.5), cp — chalcopyrite CuFeS<sub>2</sub>, (Cu/Fe = 1), tal — talnakhite Cu<sub>9</sub>Fe<sub>8</sub>S<sub>16</sub> (Cu/Fe = 1.12), mh — mooihoeikite Cu<sub>9</sub>Fe<sub>9</sub>S<sub>16</sub> (Cu/Fe = 1), hc — haycockite Cu<sub>4</sub>Fe<sub>5</sub>S<sub>8</sub> (Cu/Fe = 0.8).

**Abstracts**

**Table 2.** Composition of phases synthesized in this study and natural chalcopyrite solid solution crystallization products

Phases	Composition of phases, wt. %			Source
	Cu	Fe	S	
Isocubanite (cb)	23.92–26.78	38.70–40.17	34.22–34.46	This study, with cp, with hc. <i>Missack et al., 1989</i> <i>Mozgova et al., 1995, 2002</i> <i>Distler et al., 1996</i>
	19.59–23.34	41.57–44.03	34.42–35.25	
	22.23	41.98	35.79	
	19.25–23.40	37.60–43.80	34.30–37.52	
	18.10–24.94	34.46–41.73	34.20–36.70	
Chalcopyrite (cp)	28.03–34.97	31.07–36.96	4.37–34.38	This study, with cb, With cb and with tal. <i>Karpenkov, 1974</i> <i>Distler et al., 1996</i> <i>Phardust et al., 2005</i> . Lamelle from exsolution textures
	33.40–34.86	29.76–32.03	34.34–34.38	
	30.2–32.0	33.2–34.9	33.8–35.7	
	26.54–31.37	31.98–36.56	33.74–35.66	
	31.23–34.17	27.87–32.36	35.06–36.03	
32.63–33.21	31.42–31.85	34.98–35.64		
Isochalcopyrite	33.1–35.3	31.4–32.4	33.2–34.1	<i>Philimonova et al., 1974</i> <i>Missack et al., 1989</i> <i>Phardust et al., 2005</i> . Lamelle from exsolution textures
	34.04	32.20	33.87	
	31.69	34.51	33.85	
	33.08	32.81	33.88	
Talnakhite (tal)	36.64–37.68	28.75–29.13	32.74–33.42	This study. <i>Budko, Kulagov, 1963</i> <i>Cabri, Hall, 1972</i> <i>Philimonova et al., 1974</i>
	36.5–8.6	29.5–32.0	31.0–32.0	
	36.86–37.36	28.79–29.47	33.06–33.84	
	36.8	29.8	34.0	
Mooihoekite (mh)	34.74–37.18	31.46–32.83	31.68–32.25	This study. <i>Cabri, Hall, 1972</i> <i>Philimonova et al., 1974</i>
	34.87–36.71	31.38–32.40	31.93–33.29	
	35.3–36.2	31.4–31.9	32.1–32.9	
Haycockite (hc)	30.65–34.71	33.06–38.32	31.43–32.91	This study. <i>Cabri, Hall 1972</i>
	31.83–32.55	34.64–35.46	31.94–32.86	

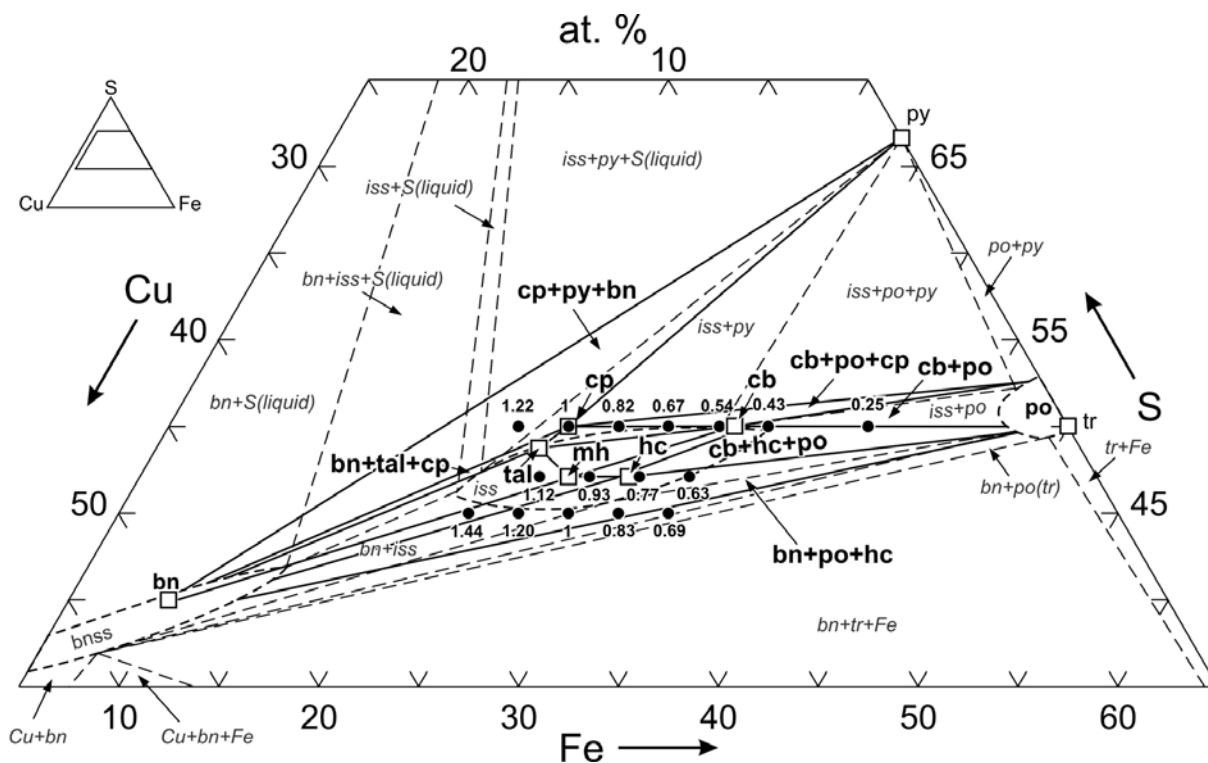


**Fig. 1.** The relations scheme of synthesized phases (solid lines) in the scheme of phase relationships of the central part of the Cu–Fe–S system at 600 °C (dashed lines, [Cabri, 1973]). • — the initial compositions of synthesized samples: 50 at.% S, Cu/Fe 1.22–0.25; 47 at.% S, Cu/Fe 1.12–0.63; 45 at.% S, Cu/Fe 1.44–0.69. The iss, bnss and po notations represent regions of chalcopyrite, bornite and pyrrhotite solid solutions correspondingly. The □ symbol shows stoichiometric compositions of the following minerals: CuFeS<sub>2</sub> (cp), bornite Cu<sub>5</sub>FeS<sub>4</sub> (bn), pyrite FeS<sub>2</sub> (py), troilite FeS (tr) and chalcopyrite solid solution products: chalcopyrite CuFeS<sub>2</sub>, talnakhite Cu<sub>9</sub>Fe<sub>8</sub>S<sub>16</sub> (tal), cubanite CuFe<sub>2</sub>S<sub>3</sub> (cb), mooihoekite Cu<sub>9</sub>Fe<sub>9</sub>S<sub>16</sub> (mh) and haycockite Cu<sub>4</sub>Fe<sub>5</sub>S<sub>8</sub> (hc).

**Mooihoekite.** Composition of mooihoekite with Cu/Fe = 1.04 – 0.93 corresponds to the bornite (bn) – mooihoekite (mh) - cubanite (cb) equilibrium line, which crosses the chalcopyrite and haycockite phase associations regions.

**Cubic pc haycockite.** The iron-enriched isocubanite is crystallized in associations with pyrrhotite and haycockite. As opposed to natural rhombic haycockite, synthetic phase of haycockite composition is characterized by cubic pc structure [Cabri, 1973]. Cubic pc structure has been determined for phases of 46–48 at.% S, Cu/Fe = 1–0.68 synthesized in the given study. Cubic pc haycockite (Cu/Fe = 0.92–0.68) is crystallized in the associations: pyrrhotite + iron-enriched isocubanite (Cu/Fe = 0.49–0.39) and pyrrhotite + bornite. As shown in the table 1 the similar total range of the Cu/Fe value for mooihoekite and haycockite (1.04–0.68) and for chalcopyrite (1.03–0.67) has been determined.

The compositions of synthesized phases correspond to published data about compositions of the appropriate minerals (table 2).

Thereby formation of the phase relations in the central part of the Cu-Fe-S system is determined by the initial composition and cooling regime of the melt. Pyrrhotite + iron-enriched isocubanite (Cu/Fe = 0.49–0.39), stoichiometric isocubanite (Cu/Fe = 0.52–0.49) and copper-enriched isocubanite (Cu/Fe = 0.61–0.52) + chalcopyrite (Cu/Fe = 0.99–0.67) are crystallized from the melt with 50 at.% S. When decreasing the sulphur content the composition of the following phase associations is changed: pyrrhotite + isocubanite → pyrrhotite + isocubanite + haycockite (Cu/Fe = 0.90–0.68) → pyrrhotite + haycockite (Cu/Fe = 0.92–0.68) + bornite, isocubanite → isocubanite + mooihoekite (Cu/Fe = 1.04–0.93) + bornite, isocubanite + chalcopyrite → isocubanite + talnakhite (Cu/Fe = 1.16–1.09) + chalcopyrite (Cu/Fe = 1.03–0.92).

#### References:

1. Bud'ko, I. A., E. A. Kulagov (1963). Natural cubic chalcopyrite, *Doklady Earth Sciences*, T. 152, No 2 (in Russian).
2. Cabri, L. J., S. Hall (1972). Mooihoekite and haycockite, two new copper-iron sulfides, and their relationship to chalcopyrite and talnakhite, *Amer. Mineralogist*, v. 57, pp. 5–6.
3. Cabri, L. J. (1973). New data on phase relations in the Cu-Fe-S System, *Economic Geology*, v. 68, pp. 443–454.
4. Distler, V. V., E. A. Kulagov., S. Ph Slujenikin, I. P. Laputina (1996). Hardened sulfide solid solutions in the ores of Noril'sk deposit, *Geology of Ore Deposits*, v. 38, No 1, pp. 41–53 (in Russian).
5. Karpenkov, A. M., G. A., Mitenkov, N. S. Rudashevski (1974). Iron-enriched form of chalcopyrite, *ZVMO*, part. 103, issue 1 (in Russian).
6. Kravchenko, T. A., E. N. Nigmatulina (2009). Experimental study of Au and Ag phases during crystallization of Cu–Fe sulfide melt, *New Data on Minerals*, Moscow: EKOST, issue 44, pp. 56–65 (in English, in Russian).
7. Kravchenko, T. A. (2009). Pt–Pd–Sn intermetallik compounds crystallized from Cu-Fe sulfide melt, *New Data on Minerals*, Moscow: EKOST, issue 44, pp. 66–73 (in English, in Russian).
8. Kravchenko, T. A. (2011). Experimental study of the phase equilibria during the crystallization region of the chalcopyrite solid solution, *New Data on Minerals*, Moscow: EKOST, issue 46, pp. 86–92 (in English, in Russian).

9. Missack, E., P. Stoffers, A. Goresy (1989). Mineralogy, parageneses and phase relations of copper iron sulfides in the Atlantis II deep, Red Sea, *Mineral Deposit*, issue 24, pp. 82–91.
10. Mozgova, N. N., S. N. Nenasheva, Yu. S. Borodaev, A. I. Cepin (1995). Region of the chalcopyrite composition and characteristics of the isocubanite isomorphism, *Geochemistry*, No 4, pp. 533 – 551 (in Russian).
11. Mozgova, N. N., Yu. S. Borodaev, I. Ph. Gablina, G. A. Cherkashev, T. V. Stepanova, E. A. Jirnov (2002). Izokubanit from sulfide ores of the Rainbow hydrothermal field (Mid-Atlantic Ridge, 36 ° 14 N), *ZVMO*, No 5 (in Russian)
12. Phardust, Ph., N. N. Mozgova, Yu. S. Borodaev, N. I. Organova, L. A. Levickaya (2005). Easily oxidizable chalcopyrite from Rainbow hydrothermal field, *New Data on Minerals*, Moscow: EKOST, V. 40.
13. Philimonova, A. A., I. V. Muraveva, T. L. Yevstigneeva (1974). The chalcopyrite group minerals in the Cu–Ni ores of Noril'sk deposits, *Geology of Ore Deposits*, No 5, pp. 36–46 (in Russian).
14. Sugaki A., H. Shima, A. Kitakaze, H. Harada (1975). Isothermal phase relations in the system Cu–Fe–S under hydrothermal conditions at 350 °C and 300 °C, *Economic Geology*, V. 70, pp. 806–823.
15. Tsujimura T., A. Kitakaze (2004). New phase relations in the Cu–Fe–S system at 800°C; constraint of fractional crystallization of sulfide liquid, *N. Jb. Miner. Mh*, 10, pp. 433–444.
16. Yund R. A., G. Kullerud (1966). Thermal stability of assemblages in the Cu–Fe–S system, *Jour. Petrology*, V. 7, pp. 454–488.

#### Marina E.A., Marin A.A., Mahina I. B., Balitsky V. S. Experimental study of bismuthous minerals crystallization

Institute of Experimental Mineralogy RAS, Chernogolovka  
[marina@iem.ac.ru](mailto:marina@iem.ac.ru)

The paper presents results of experimental researches on the synthesis and study of the morphology of bismuthous minerals such as eulytite, sillenite, and bismite. These minerals are extremely rare in nature as well-formed crystals, so the study of their morphology is preferable to synthetic analogues.

*Key words:* bismuth minerals, hydrothermal synthesis

**Reference:** Marina, E. A., A. A. Marin, A. B. Makhina, V. S. Balitsky. (2012), Experimental study of bismuthous minerals crystallization, *Vestnik ONZ RAS*, 4, (

Bismuth is rare element. It occurs in nature in the form of numerous minerals, mainly of hydrothermal origin, the principal of which are: bismuthinite or bismuth luster (Bi<sub>2</sub>S<sub>3</sub>), native bismuth (Bi), bismite or bismite ocher (Bi<sub>2</sub>O<sub>3</sub>), tetradymite (Bi<sub>2</sub>Te<sub>3</sub>), etc. These minerals are scattered and occur as impurities in the lead-zinc, copper, molybdenum-cobalt and tin-tungsten ores. The deposits of its own ores of bismuth are rare and relatively small in scale. As an exception may be called industrial clusters of native bismuth in the Ore Mountains (Eastern Germany), Bolivia and Australia. There are about 90 bismuth minerals, but the industrial importance has only a few of them.

We have carried out experimental studies to the synthesis of bismuth minerals such as bismite (Bi<sub>2</sub>O<sub>3</sub>), sillenite (Bi<sub>12</sub>M<sub>x</sub>O<sub>20 ± δ</sub>) and eulytite (Bi<sub>4</sub>(SiO<sub>4</sub>)<sub>3</sub>). The studied minerals are extremely rare in nature, especially in the form of well-formed crystals, so the growth and study

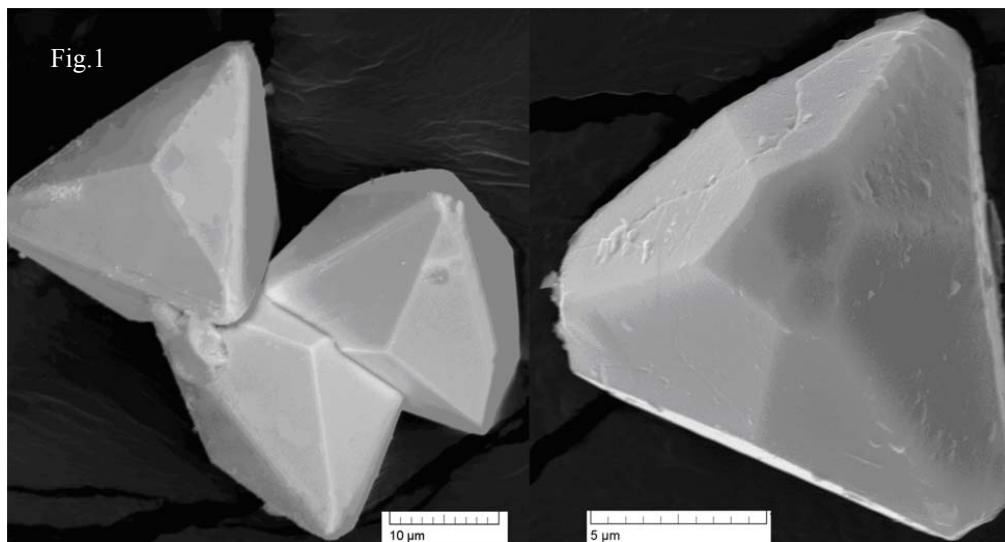


Fig. 1. Eulytite crystals grown in a 5% solution of hydrogen peroxide (photo by scanning electron microscopy)

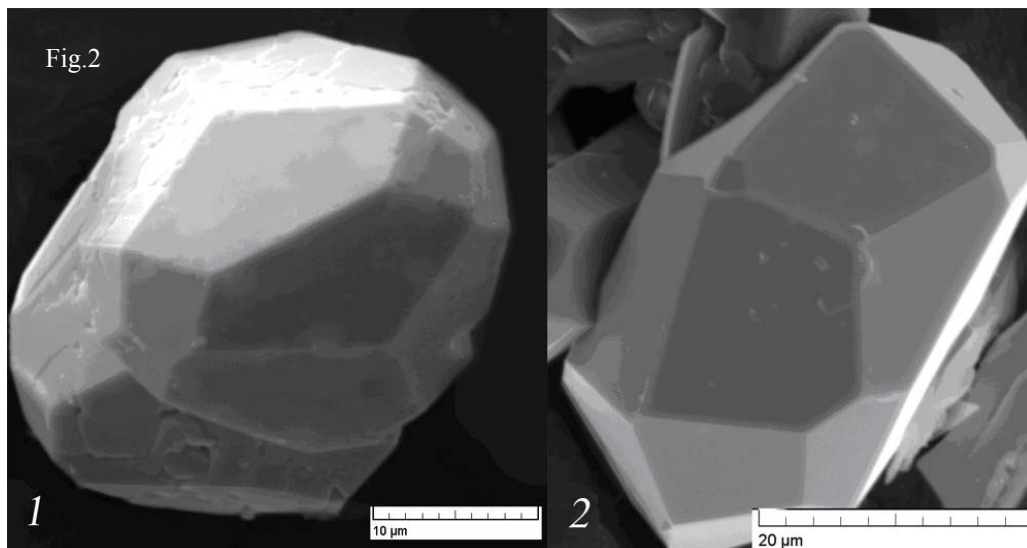


Fig. 2. Eulytite crystals grown in 1 – NaOH and 2 – NH<sub>4</sub>F solutions (photo by scanning electron microscopy)

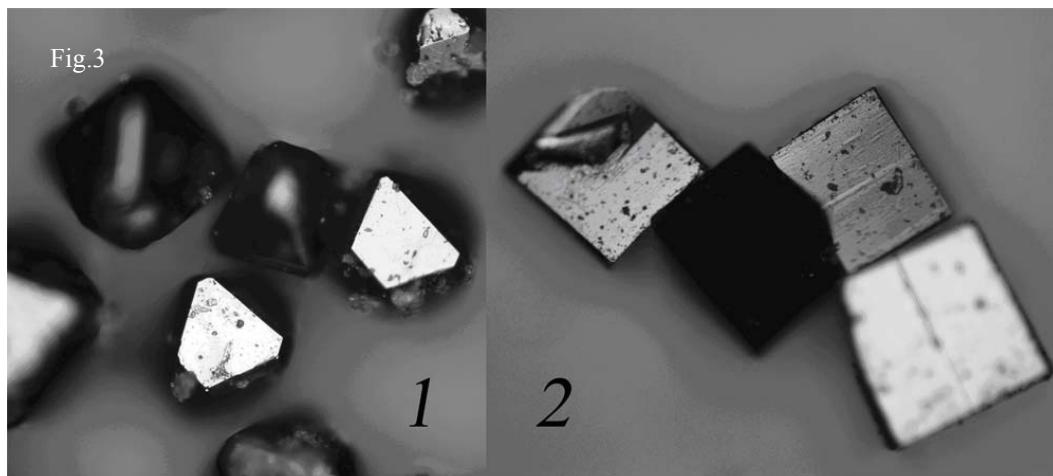


Fig. 3. 1 – gallium sillenite crystals, 2 – phosphorous sillenite (photo by optical microscope)

of their morphology is a very urgent task. In addition, bismuthous minerals have a number of important technical features: scintillation (eulytite) and piezoelectric

Teflon fettle. The autoclave was filled with the same solution with the same factor of filling as ampoules. As the charge was used Bi<sub>2</sub>O<sub>3</sub> or NaBiO<sub>3</sub>. In addition, to the charge placed various additives C<sub>4</sub>H<sub>10</sub>O<sub>6</sub>Zn, Ga<sub>2</sub>O<sub>3</sub>, Fe<sub>2</sub>O<sub>3</sub>,

(sillenite), which determines the relevance of research in this area.

The method of hydrothermal synthesis of bismuthous minerals included the preparation of autoclave equipment, preparation of the solution and the charge and direct experimentation. Growth was carried out at relatively low parameters of temperature and pressure (temperature of 250–260 ° C, pressure 500 bar).

Eulytite crystals synthesized in aqueous solutions of NaOH (15%), NH<sub>4</sub>F (1–5%), and (for the first time in the world) in solutions of hydrogen peroxide H<sub>2</sub>O<sub>2</sub> (2–10%). Growth was carried out in high-temperature autoclaves of 50 and 225 ml, from stainless steel and Cr-Ni alloy. Use of contact Teflon fettle was feature of the technique applied by us, allowing excluding ingress of the elements containing in a steel of autoclaves in a solution. As an initial charge used powdered chemicals Bi<sub>2</sub>O<sub>3</sub> (84 wt.%) And SiO<sub>2</sub> (16 wt.%).

Sillenite crystals were grown up in 10% solution of NaOH. Synthesis was carried out in Teflon ampoules in volume of 5–8 ml, which in the amount of six pieces was placed in a high-temperature autoclave also with

SiO<sub>2</sub>, Na<sub>3</sub>PO<sub>4</sub> · 12H<sub>2</sub>O, K<sub>2</sub>CrO<sub>3</sub>, Al(OH)<sub>3</sub>, Bi<sub>2</sub>O<sub>3</sub> or NaBiO<sub>3</sub> were 95% of the total mass of the charge, and one of the above additives of 5%.

Bismite formed as a by-product at the synthesis of eulytite and sillenite in NaOH (10–15%) solutions. In the absence of sillenite-formative additives bismite formation is 100%.

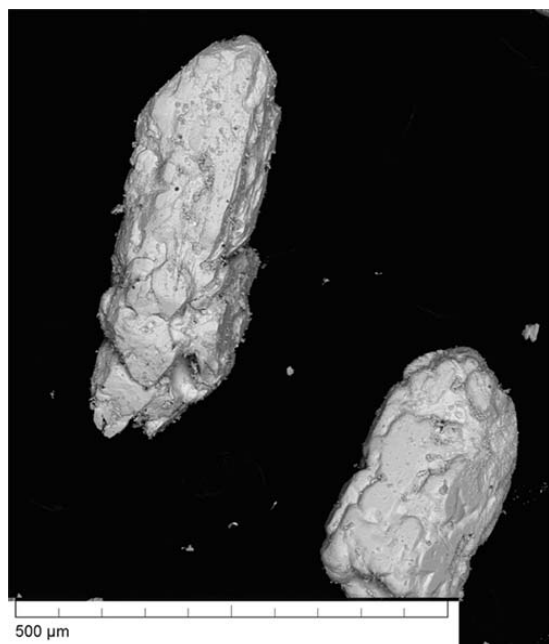


Fig. 4. Bismite crystals (photo by scanning electron microscopy)

The initial charge with the necessary additives placed on the bottom of the autoclave (in amount 5–10 g) or in an ampoule (in amount 1 g), further solution with factor of filling 0.85 (that at temperature 260°C create in the autoclave pressure of an order the 500th bar) was filled in. Charged thus autoclaves was hermetically closed and placed in an electric resistance furnace. Duration of experiments was from 2 to 20 days. At the end of the experiments autoclaves were opened, the contents of the fettle were taken and the process of separating the synthesized crystals from the crystallization medium began.

The obtained crystals were investigated by means of a digital scanning electron microscope Tescan VEGA II XMU with dispersion spectrometer INCA wave 700, by diffractometer DRON-"g" (Co-radiation, iron filter) and by optical microscope Nikon Eclipse LV 100 POL.

Eulytite crystals grown in different solutions (NaOH, NH<sub>4</sub>F, H<sub>2</sub>O<sub>2</sub>) have tetrahedral habitus, but generally that's crystals aggregates with vague marked faces. The crystals that were grown in hydrogen peroxide were most analogous to natural eulytite.

Sillenite crystals grown in NaOH, have trigonal-tritrahedral habitus. Faces of crystal {100} and {110} are most developed. Since the sillenite occurs as fine-grained earthy masses in the nature, the study of his habitus expedient to carry out on synthetic crystals.

We have synthesized zinc-, gallium-, iron-, silicon-, phosphorus- and chromium-containing sillenite crystals in the size of 0.1–0.5 mm. Zinc-, gallium-, iron- and chromium-containing crystals are usually formed as a tetrahedron, and the silicon- and phosphorus-sillenites as a cube.

Bismite Bi<sub>2</sub>O<sub>3</sub> crystallizes in the monoclinic syngony. Bismite crystals are pseudorhombic, aggregates are fine-

grained and powdery, in nature usually occurs as crusts on the native bismuth. We was synthesized bismite in NaOH. Bismite crystals are pseudorhombic, faces badly formed.

The carried-out researches was allowed to obtain of synthetic crystals of the bismuthous minerals which extremely rare in nature, and also to study their habitus.

#### References:

1. Glembotskiy, V. A. et al (1972). Bismuth: Enrichment of bismuthous-ore, Dushanbe: Donish, p. 150
2. Kargin, Y. F., et al (2004). Sillenite crystals. Synthesis, structure, properties, Moscow, Azbuka- 2000, p. 316
3. Marin, A. A. (1982). The use of hydrothermal synthesis method for the study of crystal-chemical characteristics of sillenite. In the book: Problems in the experimental solid-state and hydrothermal high-pressure apparatus, Moscow, Science, p.214-219

#### Martynov <sup>1</sup>K. V., Lapitskaya <sup>1</sup>T. S., Tananaev <sup>1</sup>I. G., Kovalsky <sup>2</sup> A. M. Limits of replacement of Zr and Ti for Al in kosnarite solid solution including alkali and alkaline earth charge-compensating cations

<sup>1</sup>A. N. Frumkin Institute of Physical Chemistry and Electrochemistry RAS, Moscow

<sup>2</sup>Institute of Experimental Mineralogy RAS, Chernogolovka  
[mark0s@mail.ru](mailto:mark0s@mail.ru)

Limits of replacement of framework forming octahedral cations: Ti<sup>4+</sup> and Zr<sup>4+</sup> for Al<sup>3+</sup> in kosnarite were studied by a method of high-temperature solid phase synthesis at atmospheric pressure. Influence of various types of replacements in solid solution Me<sup>n+</sup><sub>(1+x)/n</sub>Al<sub>x</sub>(Ti,Zr)<sub>2-x</sub>(PO<sub>4</sub>)<sub>3</sub>, where Me<sup>n+</sup> is Na<sup>+</sup>, K<sup>+</sup>, Cs<sup>+</sup>, Ca<sup>2+</sup>, Sr<sup>2+</sup>, Ba<sup>2+</sup>, for the sizes of a crystal cell and limitations of an isomorphous substitutions within kosnarite structure were interpreted by the crystal-chemical analysis.

*Key words:* kosnarite, solid solution, isomorphism, crystal-chemical analysis.

**Citation:** Martynov, K. V., T. S. Lapitskaya, I. G. Tananaev, A. M. Kovalsky (2012), Limits of replacement of Zr and Ti for Al in kosnarite solid solution including alkali and alkaline earth charge-compensating cations, *Vestn. Otd. nauk Zemle*, 4,

The mineral kosnarite, opened two decades ago, on a chemical composition is complex orthophosphate KZr<sub>2</sub>(PO<sub>4</sub>)<sub>3</sub> and crystallizes in a trigonal crystal system (s.g. R -3 c, Z=6). Thanks to the properties, synthetic analogs of kosnarite were known long before its discovery. NaSiCon (Na<sub>1+x</sub>Zr<sub>2</sub>Si<sub>x</sub>P<sub>3-x</sub>O<sub>12</sub>) was studied as solid electrolytes, and NZP (NaZr<sub>2</sub>(PO<sub>4</sub>)<sub>3</sub>) – as matrixes for components of radioactive waste and catalysts for organic synthesis. Thus, kosnarite is natural analogue of the most important in the technological relation of chemical compounds just as a pyrochlore, a perovskite, zeolites and other mineral types. Therefore, as it is accepted in other cases, all compounds and solid solutions having kosnarite's chemical composition and structure, we will call his name.

Despite simplicity of a chemical composition given above compounds, kosnarite represents the multicomponent solid solution possessing wide isomorphism of all types of cations entering into it. Its crystal-chemical formula can be presented as

## Abstracts

$(^{VI}M1)(^{VIII}M2)_3\{^{VI}L_2(^{IV}TO_4)_3\}$ , where  $^{IV}T$  is framework forming tetrahedral cations with charge  $n = +4 - +6$ : Si, Ge, Sn, P, V, As, Sb, S, Se, Mo, etc.,  $^{VI}L$  is framework forming octahedral cations with charge  $n = +3 - +5$ : Al, Ga, In, Cr, Fe, Ti, Zr, Hf, Nb, etc. These two types of polyhedra ( $TO_4$  and  $LO_6$ ), linking by corner atoms of oxygen, built the three-dimensional framework possessing a negative charge which is compensated by the cations located in  $^{VI}M1$  and  $^{VIII}M2$  cavities of a framework.  $^{VI}M1$  position is preferable and only after its settling, cations occupy  $^{VIII}M2$  position. Thus, extra frame positions can be vacant ( $\square$ ) or are occupied with cations with charge  $n = +1 - +4$ , for example: alkali, alkaline earth, rare-earth metals, actinides, etc.

$x)_{1/m}L_2(TO_4)_3$ , where the end-member fraction changes within  $X=0-1$ . Replacement of cations being in a tetrahedral position is described by reaction:  $kT^{n+}+(n-m)\square=kT^{m+}+(n-m)M^{k+}$ , crystal-chemical formula is  $M^{k+}_{\{3(5-n)+X(n-m)+1\}/k}L_2T^{m+}_X T^{n+}_{3-X}O_{12}$ , where  $X=0-3$ . At last, isomorphism of octahedral cations -  $kL^{n+}+(n-m)\square=kL^{m+}+(n-m)M^{k+}$ , crystal-chemical formula is  $M^{k+}_{\{2(4-n)+X(n-m)+1\}/k}L^{m+}_X L^{n+}_{2-X}(PO_4)_3$ , where  $X=0-2$ . To compensate of a framework charge during heterovalent replacements of framework forming cations it needs to change of an extra frame vacancies/cations ratio. It also is the main mechanism of updating of composition and properties of kosnarite.

From given above reactions and crystal-chemical

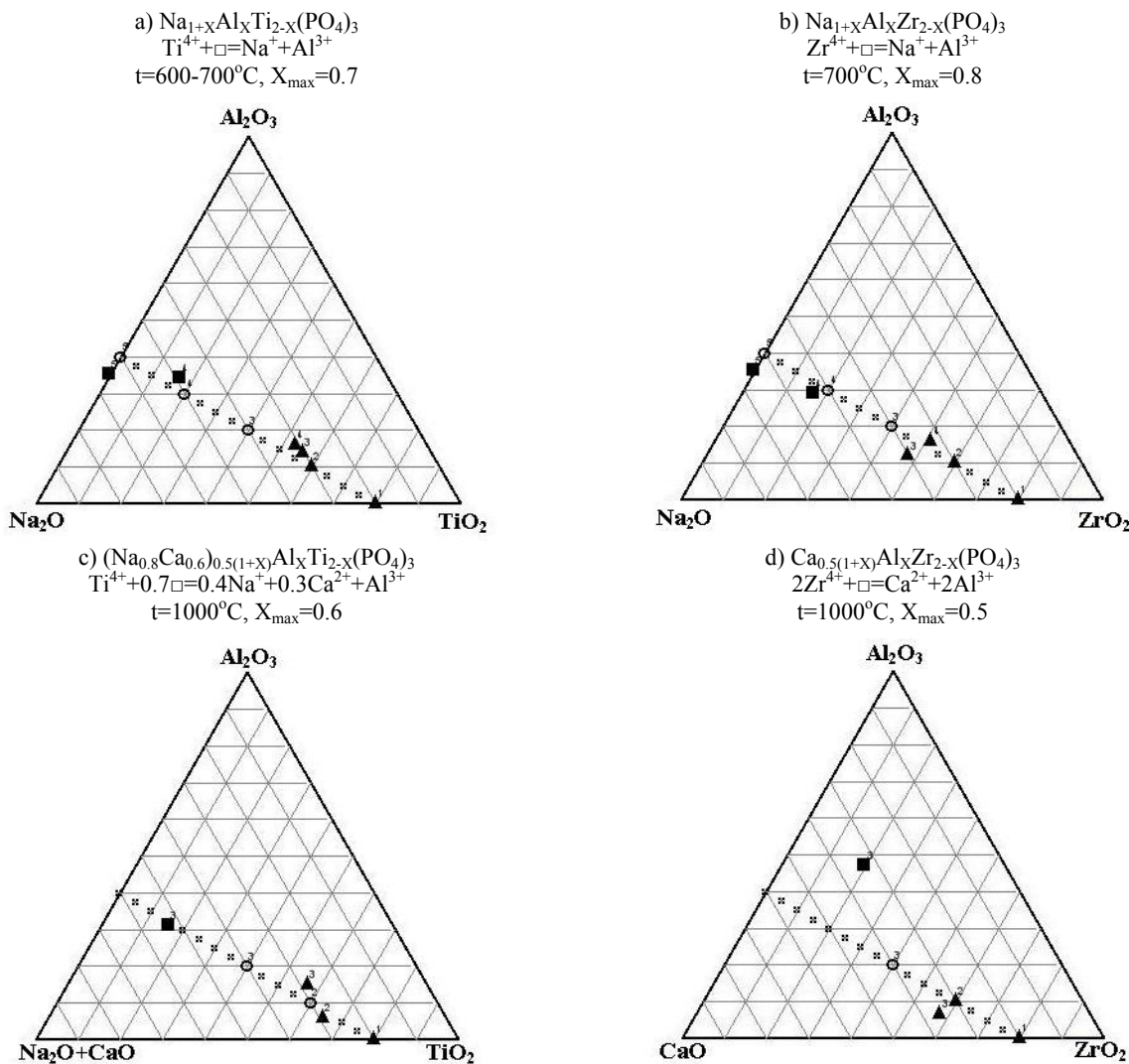


Fig. 1. Stability fields of kosnarite in the studied sections: \*\*\* – sections, o – compositions of initial mixtures, ▲ – kosnarite, ■ – tetragonal phase

Ionic conductivity, "zeolitic" properties, ability to connect toxic and radioactive elements and other useful qualities of kosnarite correlate with the nature of extra frame positions settling. Thanks to its predisposition to isomorphism it is possible to change purposefully composition and properties of kosnarite. Isomorphous replacements in kosnarite are possible in all crystal-chemical positions, and all of them can influence filling of frame cavities. First, it is actually isomorphism of extra frame cations which can be described by replacement reaction:  $mM^{n+}=nM^{m+}+(m-n)\square$ ; crystal-chemical formula of this type of solid solution is  $(M^{n+}_{(m/n)X}M^{m+}_{1-X})$ .

formulas for different types of replacements in kosnarite solid solution it is possible to find stoichiometric constraints with heterovalent isomorphism. Since the substitution of Ti or Zr for Al which is accompanied by the filling of vacancies alkali and alkaline earth charge-compensating cations according to stoichiometric constraints X can change from 0 to 2. Actually, as showed by experiments [Mouahid, 2000; Syssoeva, 2009], limiting values  $X_{max}$  are much less. For definition of replacement limits of tetravalent octahedral cations for Al we have studied four pseudo-binary sections of multicomponent system  $Na_2O-CaO-Al_2O_3-TiO_2(ZrO_2)-P_2O_5$  by a method

of high-temperature solid phase synthesis at atmospheric pressure.

Precursors for synthesis were prepared by sol-gel technique from starting reagents: NaNO<sub>3</sub>, CsNO<sub>3</sub>, Ca(NO<sub>3</sub>)<sub>2</sub>·4H<sub>2</sub>O, Al(NO<sub>3</sub>)<sub>3</sub>·9H<sub>2</sub>O, Zr(OH)<sub>4</sub> и TiOC<sub>2</sub>O<sub>4</sub>·H<sub>2</sub>O, 70% HNO<sub>3</sub>, 85% H<sub>3</sub>PO<sub>4</sub>, 25% ammonia water, over some stages: 1) dissolution and mixing for sol production, 2) gel maturing at room temperature, 3) drying at 120°C for xerogel production, 4) calcinating at 300°C for removal of the flying. Synthesis was carried out at 600-700°C for alkali kosnarites and 900-1000°C for alkaline earth ones. Products of synthesis were studied by X-ray powder diffraction (XRPD) method and electron microprobe analysis (EMPA). For phase analysis XRPD patterns of the samples have been removed on DRON-4 X-ray diffractometer, using CuKα radiation with Ni-filter (λ=1.5418 Å). For specification of crystal phases structures XRPD patterns of the samples have been removed at 25°C on Bruker D8 ADVANCE X-ray diffractometer, using CuKα<sub>1</sub> radiation (λ=1.5406 Å) with step of 0.010°2θ. In this case angular positions of reflections were corrected by the internal standard (spectral pure Si, a=5.4305 Å). CRYSFIRE 2004 (TREOR90 procedure) and CHEKCELL computer programs have been used for definition of reflection

indexes and calculation of unit cell parameters. Chemical compositions of synthesized phases have been studied by a scanning electron microscope (SEM) 1) Tescan Vega II XMU combining with X-ray energy dispersive spectrometer INCAx-sight attached with BSE+SE detectors, 2) Jeol JSM-U3 with Getac Edison-32 system, which involved WinEDS digital scanner and Eumex X-ray energy dispersive spectrometer based on Si(Li) semiconductor detector equipped with an ultrathin polymer window. For EMPA the samples have been pressed in tablets from polystyrene, polished and covered graphite.

Results of experiments on kosnarite stability in the studied sections are shown in Fig. 1, together with the parameters of the synthesis, crystal-chemical formulas of the solid solutions and substitution reactions. The stability field of alkaline earth kosnarite compounds was more limited than for the alkali ones. For X>X<sub>max</sub> decomposition of the solid solution is observed and in poor Ti or Zr field another phase crystallizes which is defined by us as a tetragonal, also forming a solid solution. Thus, the decomposition of solid solution in the studied sections was combined with the phase transition.

**Table 1.** The unit cell volumes of Ti (a) and Zr (b) kosnarites according to our and literature data and calculated values of the reduced ionic radii of extra frame cations  $R^*=(R_M^{n+}+(n-1)*R_{\square})/n$

Cation	a) $M^{n+}_{1/n}Ti_2(PO_4)_3, R_{\square}=0.53 \text{ \AA}^3$			Source for V	b) $M^{n+}_{1/n}Zr_2(PO_4)_3, R_{\square}=0.55 \text{ \AA}^3$			Source for V
	$R_{M^{n+}}, \text{ \AA}$	$R^*, \text{ \AA}$	$V, \text{ \AA}^3$		$R_{M^{n+}}, \text{ \AA}$	$R^*, \text{ \AA}$	$V, \text{ \AA}^3$	
Na <sup>+</sup>	0.95	0.95	1360	[Sysoeva, et al., 2009]	0.95	0.95	1528	[Kotelnikov, et al., 2000a]
K <sup>+</sup>	1.33	1.33	1400	[Sysoeva, et al., 2009]	1.33	1.33	1573	[Kotelnikov, et al., 2000a]
Cs <sup>+</sup>	1.68	1.68	1437	the equation shown in Fig. 2a	1.68	1.68	1582	our data
Ca <sup>2+</sup>	1.01	0.78	1341	[Sysoeva, et al., 2009]	1.01	0.78	1517	[Kotelnikov, et al., 2000b]
Sr <sup>2+</sup>	1.16	0.85	1349	[Sysoeva, et al., 2009]	1.16	0.86	1530	[Kotelnikov, et al., 2000b]
Ba <sup>2+</sup>	1.36	0.95	1359	the equation shown in Fig. 2a	1.36	0.96	1534	the equation shown in Fig. 2b

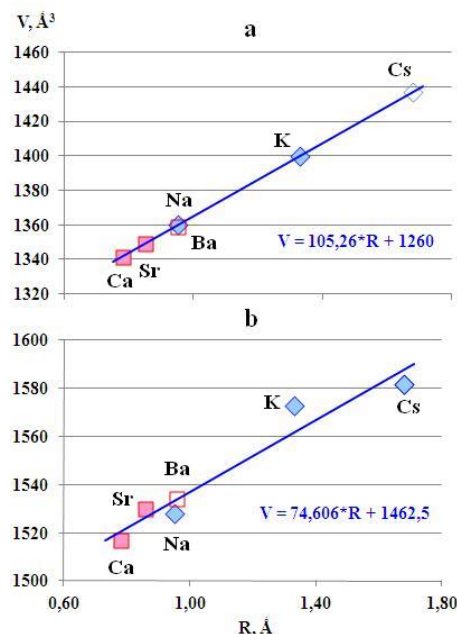


**Fig. 2.** The dependences of the unit cell volumes of  $M^{n+}_{1/n}Ti_2(PO_4)_3$  (a) and  $M^{n+}_{1/n}Zr_2(PO_4)_3$  (b) kosnarites from the reduced extra frame cation ionic radius  $R^*=(R_M^{n+}+(n-1)*R_{\square})/n$

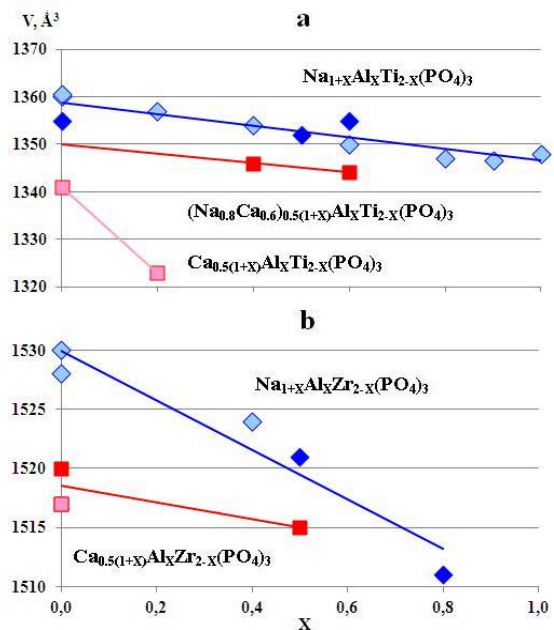


**Fig. 3.** The dependences of the unit cell volumes from the compositions of Al-containing Ti (a) and Zr (b) kosnarites according to our (filled symbols) and literature (open symbols) data

### Conclusions

Installed directly proportional dependence of the unit cell volume of kosnarite solid solution from the reduced ionic radius of extra frame cations.

Limitation of miscibility in the replacement of Ti and Zr for Al in kosnarite solid solution due to the conflict consequences of this process: the compression of the crystal structure with increasing charge of the frame on one side and a positive volume effect accompanying the replacement of the other.

Both observed effects can be used to predict the properties of kosnarite solid solution for different types of isomorphous substitution.

---

*This work was supported by The State Contract № 16.740.11.0538 from 16.05.2011.*

### References :

1. Maldonado-Manso, P. et al. (2005). Nominal vs. actual stoichiometries in Al-doped NASICONs: A study of the  $\text{Na}_{1.4}\text{Al}_{0.4}\text{M}_{1.6}(\text{PO}_4)_3$  (M=Ge, Sn, Ti, Hf, Zr) family, *Solid State Ionics*, Vol. 176, pp. 1613–1625.
2. Mouahid, F. E. et al. (2000). Crystal chemistry and ion conductivity of the  $\text{Na}_{1+x}\text{Ti}_{2-x}\text{Al}_x(\text{PO}_4)_3$
3. ( $0 \leq x \leq 0.9$ ) NASICON series, *Journal of Materials Chemistry*, No 10, pp. 2748–2753.
4. Kotelnikov, A. R. et al. (2000a). The synthesis and refinement of unit cell parameters of solid solutions of sodium-potassium zirconium phosphates:  $\text{Na}_{(1-x)}\text{K}_x\text{Zr}_2(\text{PO}_4)_3$ , *Geokhimiya*, No 10, pp. 1122–1126 (in Russian).
5. Kotelnikov, A. R. et al. (2000b). Synthesis and X-ray study of the solid (Ca, Sr)-zirconium phosphates, *Vestnik OGGGN RAN*, Vol. 1(15), No 5 (in Russian).
6. Ryabukhin, A. G. (2000). The system of effective ionic radii, *Izvestiya Chelyabinskogo nauchnogo tsentra. Fizicheskaya khimiya i tekhnologiya neorganicheskikh materialov*, No 4 (in Russian).
7. Sysoeva, T. S. et al. (2009). Synthesis and study of complex orthophosphates of alkali (alkaline earth) metals, aluminum and titanium, *Jurnal neorganicheskoy khimiyi*, vol. 54, N 6, pp. 894–904 (in Russian).